Nanoscale

Accepted Manuscript

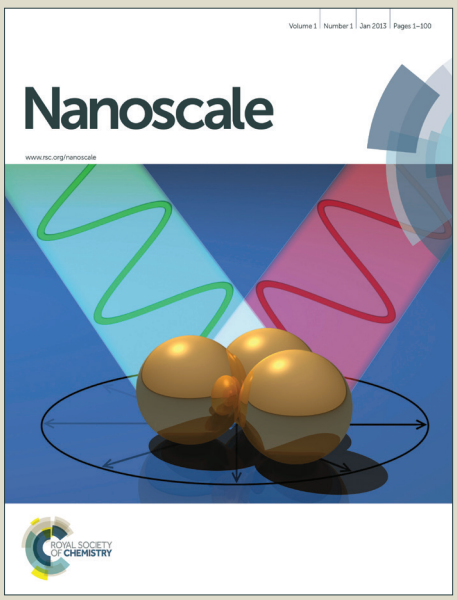

ROYAL SOCIETY OF CHEMISTRY

www.rsc.org/nanoscale

Nanostructured pseudocapacitive materials decorated 3D graphene foam electrodes for next generation supercapacitors

Umakant Patil‡, Su Chan Lee‡, Sachin Kulkarni‡, Ji Soo Sohn, Min Sik Nam, Suhyun Han, Seong Chan Jun*

Nano-Electro Mechanical Device Laboratory, School of Mechanical Engineering, Yonsei University, Seoul 120-749, South Korea.

Abstract

Nowadays, advancement in performance of proficient multifarious electrode materials conclusively lies as the core of research concerning the energy storage devices. To accomplish superior capacitance performance the requirements of high capacity, better cyclic stability and good rate capability can be expected from integration of EDLCs based carboneous materials (high power density) and pseudocapacitive based metal hydroxides/oxides or conducting polymers (high energy density). Envision of three dimensional (3D) graphene foam are predominantly advantageous to extend the potential applicability by offering large active surface area and highly conductive continuous porous network for fast charge transfer with decoration of nanosized pseudocapacitive materials. In this article, we review the latest methodologies and performance evaluation for 3D graphene based several metal oxides/hydroxides and conducting polymers electrodes with improved electrochemical properties for next generation supercapacitors. The most recent research advancements of our and others group in the field of 3D graphene based electrode materials for supercapacitor are discussed. In the interest of recovering problems a careful interpretation and rigorous scrutinizing of the electrochemical characteristics of any studied materials is essential. Auspiciously, both nano-structuration as well as confinement of metal hydroxides/oxides and conducting polymers onto a conducting porous 3D graphene matrix play a great role in improving the performance of electrodes mainly due to (i) active material access over large surface area with fast charge transportation (ii) synergetic effect of electric double layer and pseudocapacitive based charge storing.

Keywords: 3D graphene foam (3D GF), Pseudocapacitive materials (PCMs), Preparation methods, Structural and morphological studies, Supercapacitors.

Corresponding Author:

Dr. S. C. Jun*

*Email: scj@yonsei.ac.kr, Tel: +82-2-2123-5817, Fax: +82-2-312-2159.

‡ These authors contributed equally

1. Introduction

Currently, development of cost-effective, maintenance-free, highly efficient, and environmentally friendly energy storage systems are in increasing demand due to use of fossil fuels, environment pollution, global warming, and rapid resource depletion [1]. Among various energy storage devices, supercapacitors are very attractive due to their high specific power (>10 kW kg^{-1}) and moderate specific energy (~10 Wh kg^{-1}). These characteristics generally meet the growing demand for time-dependent electric power systems for portable electronics, hybrid electric vehicles (HEVs), power tools, stop-and-go systems, and others [2, 3]. Generally, three major types of materials used in supercapacitor devices: carbon materials, transition metal oxides/hydroxides and conducting polymers.

Carbon based materials, such as carbon nanotubes (CNTs) [4-7], activated carbon (AC) [8-10], and graphene nanosheets (GNS) [11-13], can store energy by ion adsorption on the surface of carbon (electrochemical double layer capacitors, EDLCs) [14]. Porous carbonaceous materials are regarded as EDLC supercapacitors, where surface area, pore structure, and conductivity of electrodes are critical parameters [15]. Recently, graphene has attracted great attention due to its special structure, unique properties in chemistry, physics and mechanics. Graphene is a two-dimensional one-atom-thick planar sheet of sp^2 bonded carbon atoms, which is considered as the fundamental foundation for all fullerene allotropic dimensionalities (carbon nanotube, fullerene, diamond). Graphene is a planar monolayer of carbon atoms arranged into a two-dimensional (2D) honeycomb lattice with a carbon–carbon bond length of 0.142 nm [16, 17]. Electrons in graphene behave like massless relativistic particles, which contribute to very peculiar properties such as an anomalous quantum Hall effect and absence of localization [18, 19]. Graphene has demonstrated a range of exciting properties including high mechanical flexibility (Young's modulus of 1.0 TPa), large surface area (~2630 m^2 g^{-1}), and chemical stability with superior electric conductivities (carrier mobility up to 10,000 cm^2 V^{-1} s^{-1}) [20-25]. Particularly, high surface is important characteristic of an electrode material in energy storage devices, and theoretical surface area of graphene was reported to be ~2630 m^2 g^{-1}, surpassing that of both single wall carbon nanotubes (SWCNTs) and graphite which are reported to be ~1315 m^2 g^{-1} and ~10 m^2 g^{-1}, respectively [22]. Additionally, electrical conductivity of graphene, resulting from its extensive conjugated sp^2 carbon network, reported to be ~64 mS cm^{-1} that is approximately ~60 times higher than that of SWCNTs [22], and it remains stable over a wide range of temperatures; essential for reliability in many energy related applications [23-25]. All these excellent typical properties of graphene render it a great choice as electrode material for

EDLC based supercapacitors.

However, EDLC based energy storage devices exhibits low specific capacitance (SC), which cannot meet emerging requirements for devices that demand high energy [26]. Subsequently, there has been growing interest in pseudocapacitive materials (PCMs) for energy storage devices with high energy density, which is larger at least by one magnitude than EDLCs [26-28]. The transition metal hydroxides/oxides and conductive polymers with multiple oxidation states are usually used as pseudocapacitive energy storage materials, that possess an excellent redox reactions [29]. All polymorphs (e.g. α, β and γ) of metal oxides/hydroxides and conducting polymers are typical PCM's that can achieve relatively high capacitance [30-37]. These PCMs have been renowned as most promising material due to their high theoretical specific capacitance (>1000 F g^{-1}) [38]. However, poor electrical conductivity of metal oxides/hydroxides and deprived cyclability of polymers, due to structural degradation of electrode during redox process, are the obstacles for their application as supercapacitor electrodes [39-42].

In efforts to improve electrochemical performance of PCMs-based electrodes in supercapacitors, its various nanostructures and composites with carbon material (comprising high surface area with good conductivity) have been studied [41-47]. Recently, porous and light weight graphene materials, 3D graphene foams (GF) have been studied due to their unique inherent properties; porous structure have a higher surface area and much more "space" for transportation or storage of electron/ion and electrolyte [48]. In comparison with original graphene sheets, porous graphene materials have possessed outstanding properties for applications in electrochemical energy storage devices (supercapacitors, batteries, fuel cells, etc.), solar cells (DSSCs), gas sensors, glucose sensor, thermal transport, and oil absorption (few of them are shown in Figure 1) [49-56]. Continuous conducting structure and being lightweight (~20 mg cm^{-3}), make GF promising candidate as substitute to conventional current collectors such as nickel foam (NF) (~262 mg cm^{-3}) or carbon paper in energy storage devices.

This feature article narrates brief history of recent research progress on synthesis and properties of nanostructured PCMs on 3D porous GF. Their advantages and disadvantages are compared and summarized according to available literature to date. In addition, new trends in materials development have also been proposed in concerns with their application in supercapacitor.

2. Fabrication of graphene foam 3D architectures

On the basis of above considerations, there has been need to design and construct energy storage devices that can provide high energy and power to accomplish emerging demand of portable electronic devices. Recently, PCMs' enchased porous 3D GF electrodes are gaining interest in energy storage devices due to its unique advantageous architecture. The GF electrode is 3D graphene architecture, and can be made by chemical-assembling 2D GNS as building blocks or template assisted chemical vapour deposition (CVD) method.

2.1 Chemically assembled 3D graphene foams from graphene nanosheets (GNS)

Since graphene was discovered by mechanical exfoliation using Scotch-tape in 2004, many routes have been introduced to achieve a high-quality and large-area graphene [57]. So far various fascinating strategies to produce single-layer or few-layer graphene have been reported, that can be broadly categorized as, ''top-down'' and ''bottom-up'' approaches [58]. Graphene preparation methods are important, since the properties of graphene strongly depend on preparation methods. The graphene nanosheets (GNS) can either built from separate atoms (an approach from the "bottom-up") or by various dispersion and aggregation (an approach from the "top-down") method. The "bottom-up" approaches (schematic is shown in Figure 2 (a)) are based on assembly of atoms to grow graphene. In "bottom-up" approaches, graphene sheets (GNS) directly are directly grown from organic precursors such as methane and other hydrocarbon sources by epitaxial growth [59, 60] and chemical vapour deposition (CVD) [61]. These approaches are most attractive approaches to grow high quality and large-area graphene. On the contrary, "top-down" approach (schematic is shown in Figure 2 (b)) suggests exfoliation of natural or synthetic graphite into mixture of single and few layer graphene nanosheets (GNS). The liquid-phase exfoliation [62], graphite intercalation compounds [63] and electrochemical exfoliation [64] methods are belonged to top-down approaches. These "top-down" approaches are advantageous in terms of scalable and low-cost production of GNS. Currently chemical exfoliation methods, such as Hummer's, modified Hummer's or improved Hummer's method are considered as common routes toward production of GNS by top-down approach at low cost with high yield. It first involves oxidation of well-stacked graphite, i.e. preparation of graphite oxide (GO), and is then followed by chemical reduction of GO to obtain reduced GO (rGO) [65, 66]. Oxidation results in an increase in d-spacing and intercalation between adjacent graphene layers, it weakens the interaction between adjacent sheets, and finally leads to delamination of GO in an aqueous solution. Major advantages of bulk synthesis are the formation of both GO and

rGO with controlled attachment of epoxy, hydroxyl and carboxyl species on the edges and surfaces of graphene sheets. These groups enable the formation of stable GO or rGO dispersions and easy functionalization in aqueous and organic solvents.

However, every method has its own merits and inadequacies in terms of scalability and quality of graphene. In "top-down" approaches, it is hard to obtain single-layer graphene with high quality because of defect creation during exfoliation. In particular, reduction of GO into graphene results in a graphitic structure, but it still contains large number of defects, such as nanoholes and Stone–Wales defect [67]. On the other hand, "bottom-up" approaches are extremely difficult to control manufacturing process, and thus they result in high manufacturing cost. Detailed discussion on GNS synthesis and its chemistry, physical properties can be found in several excellent review articles by Wu et al [68] and others [69-71].

a) Self-assembly of 3D graphene by chemical method

Firstly, Xu et al [72] successfully prepared mechanically strong, electrically conductive, and thermally stable self-assembled graphene hydrogel (SGH) with high specific capacitance (~160 F g^{-1}) by hydrothermal reduction of GO aqueous dispersion. In GF fabrication, SGH was prepared via a convenient one-step hydrothermal method. In typical synthesis authors used a 10 mL portion of homogeneous aqueous GO (0.5 to 2 mg mL^{-1}), sealed in a 16 mL Teflon-lined autoclave, at 180 °C for 1 to 12 h. Then autoclave was naturally cooled to room temperature and as-prepared SGHs were taken out with a tweezer and blotted with filter paper to remove surface adsorbed water. In further study, to obtain high conductivity of GF, Zhang et al [73] used a reducing agent (hydrazine or hydroiodic acid) for reduction of graphene foam. To improve mechanical strength along with conductivity of GF, Bi et al [74] demonstrated compact graphene architecture with various shapes synthesized by hydrothermal reduction (at 180 °C for ~15 h) of GO suspension using ammonia or NaOH. The authors mentioned that, proper ammonia content (pH~10.1) was beneficial for ionizing carboxyl functional groups into COO– on GO nanosheets. Combining Xu et al and Bi et al processes with some modification, Han et al [75] prepared GF with high mechanical strength with macroporous structure, by soaking GF in ammonia solution at 90 °C for only 1 h and freeze-drying at -60 °C for 72 h. Interestingly, mechanical strength of self-assembled graphene foam was greatly enhanced due to ammonia solution, the freezing point of aqueous solution was decreased and mitigated the structural damage during freeze drying, and formed covalent bonds between graphene sheets. Schematic diagram of "Self-assembly of 3D GF by chemical method" shown in Figure 3(a) which is commonly used to fabricate GF. Recently,

heteroatom-doped GNS has been gained much interest because doping can improve electrical, physical properties and can result in the enhancement in electrochemical properties. Consequently, many attempts are made by self-assembly chemical methods, in order to prepare heteroatom doped GNS based GF, fabrication details were discussed in review by Jiang et al [76].

b) Template assisted 3D graphene synthesis by chemical method

Even the self-assembly chemical methods (i.e. hydrothermal and freeze-drying methods) are simple to fabricate GF, but fail to control porous size, interconnection between sheets and conductivity. Therefore, many attempts with template assisted (PS beads and Ni foam) methods are made to fabricate GF with controlled porous structure. Choi et al [77] fabricated 3D macroporous electrodes, namely, embossed-chemically modified graphene (e-CMG) films, by using polystyrene (PS) beads as template. In the synthesis procedure, authors combined negatively charged CMGs and dispersed PS beads (2μm) in deionized water at pH 2. The PS/CMG films were produced by filtering mixed solution through anodic membrane filters (25 mm in diameter, 0.2 μm pore size, Whatman) by vacuum suction. The pH of the bath was controlled to make both components oppositely charged (CMG: negative, PS: positive), and thus stimulate electrostatic interactions between both components, leading to uniform distribution of PS particles in CMG films. The free-standing PS/CMG films were obtained by peeling them off from filter membrane (schematic is shown in Figure 3 b(i)). However, Zhang et al [78] reported facile and scalable integration of GNS on macroscopic 3D nickel foam using a self-assembly method. For fabrication of scalable GO foam, Ni foams were immersed into a 5 mg ml^{-1} GO suspension and heated at 80 °C for 10 min. Further GO was reduced via electrochemical method, the resultant product was denoted as ERGO foam, after reduction GO foam can partially restore the 2D ordered structure of graphene (see Figure 3 b(ii)). Similarly, Wang et al [79] developed 3D rGO–Ni foam as an anode for fuel cell through facile deposition of rGO sheets on nickel foam (NF). In synthesis, NF template was transferred into an autoclave (Teflon liner) filled with 25 mL aqueous GO solution and heated at 120 °C for 5 h. To reduce GO sheets and to improve the electrical conductivity, GO/NF was annealed at 400 °C in hydrogen atmosphere in a quartz tube furnace for 30 min.

Compared with general strategies, the template-directed methods offer several advantages in term of simple, efficient and low-cost, and dimensions of GF can be adjusted freely by simply adjusting templet volume, which offers great flexibility for scaling-up in practical

applications. Accordingly, many authors [79-81] have successfully developed 3D GF electrodes by coating rGO sheets onto various templates.

2.2 Template assisted 3D graphene synthesis by CVD method

The GNS and its 3D porous architecture can be prepared by hydrothermal method, freeze-drying, sol-gel method, or combined methods, but GNS would suffer from poor electrical conductivity and structural instability due to high contact resistance in inter-sheet junction. Therefore, there is a need to develop new strategies for seamlessly continuous and conductive graphene foam. Chen et al [82] prepared 3D GF by CVD method, followed by Ni etching, where NF was used as template. Similarly, with a little modification, we have fabricated 3D GF by CVD method in our lab by the following procedure. The NF (density ~480 g m^{-2}, thickness ~1.6 mm) was placed in the center of a quartz tube furnace and annealed at 1,000 ℃ for 45 min in H_2 at a pressure of 90 mTorr with a constant flow of 5 sccm of H_2 in order to reduce the oxide layers of NF. Methane (CH_4) gas was then flowed into tube while increasing pressure of hydrogen mixture to 0.45 Torr at 1,000 ℃. The concentration of carbon atoms that dissolve in the foam can be adjusted by varying ratio of CH_4 to H_2. After 45 min of CH_4 flow, quartz tube was cooled down to room temperature under protection of H_2 (90 mTorr, 5 sccm) at a cooling rate of 10 °C s^{-1}. After growth of graphene, color of NF was changed from shiny white to dark gray. To remove NF, graphene network was first coated with poly(methyl methacrylate) (PMMA) by immersing it in a PMMA solution (4.5 wt% PMMA) for several seconds followed by drying at 90 °C for 1 h. Next, the network was immersed in an etchant containing 1 mol L^{-1} $FeCl_3$ and 2 mol L^{-1} HCl at room temperature for 36 h. After removal of NF, the PMMA coated on 3D GF was removed by acetone vapor. Finally, we developed a continuous interconnected porous 3D GF (schematic of preparation procedure is shown in Figure 3 c(i)). Also, Yoon et al [83] reported SiO_2 beads assisted CVD method for 3D GF that can be mass productive with large-area coverage. GF fabrication process was followed as, annealing of PVA/Iron (Fe) precursor under H_2 environment, infiltrated into 3D-assembled-colloidal, silica reduces Fe ions and generates few-layered graphene by precipitation of carbon on the Fe surface (See Figure 3 c(ii)). Authors have grown 3D-GF on many electronic device-compatible substrates, such as Al_2O_3, Si, GaN and Quartz. Template assisted CVD method for GF fabrication is advantageous in terms of conductivity, well-interconnected structure. Therefore, Yi et al [84] and others [76] did many similar attempts for the synthesis of porous GF using SiO_2 beads as template for CVD method.

3. Pseudocapacitive materials (PCMs) decorated 3D Graphene foam for supercapacitor

Recent progress on PCMs-graphene composites as advanced electrode materials for electrochemical energy storage devices (ECs) were described and highlighted in many research articles [85-87]. It is well known that importance of synergistic effects between graphene and PCMs with beneficial role of graphene in composites for energy storage devices. It was demonstrated that, when PCMs-graphene composites are used as electrode materials for energy storage, compared to their individual constituents, composites have a significant improvement in their electrochemical properties such as high capacity, high rate capability and excellent cycling stability [86, 87]. However, conventional architectures of PCM-graphene electrodes offer self-dimensional restrictions in charge transportation during charge-discharge process. So, new architecture of PCMs/GF electrodes gaining much consideration in the energy storage device application because of their porous and conducting structure, it provides easy charge transportation and effective utilization of PCMs with high surface area. Recently, many researchers apply 3D GF electrodes in various applications as shown in Figure 1, however, this feature article focuses mainly on PCMs/3D GF electrodes for supercapacitor applications.

3.1 Decoration of PCMs on 3D graphene foam

Since, 3D GF has promising suitability in the electrochemical field as every atom is a surface atom in a graphene sheet, thus molecular interactions and electron transport through graphene can be exceedingly sensitive to adsorbed molecules. In this regard, it is assumed that graphene will show greater capability in charge transport and storage mechanisms than conventional electrodes. These reinforcing characteristics open up great interest in developing multifunctional graphene-based electrode materials. Based on above considerations, many nanostructures of PCMs decorated on 3D GF electrodes (shown in Figure 4(a)) for supercapacitor application. The PCMs can be decorated on 3D GF by chemical and electrochemical methods e.g., hydrothermal, solution growth and electrochemical deposition method. Chemical and electrochemical deposition methods are based on efficient “bottom-up” approaches to grow various nanostructures on GF. The nanostructured PCMs growth on graphene skeleton can be explained by growth mechanism of ‘self-assembly’ and ‘oriented attachment’ processes [88]. The formation of PCMs can be explained in two steps, (a) formation of nuclei on graphene surface by ‘self-assembly’ process, (b) further nanostructures tend to grow by ‘oriented attachment’ process, schematic of growth mechanism is shown in Figure 4(b). In the growth process of 3D GF, some wrinkles and defects form on the surface

of graphene skeleton due to grain boundaries of Ni. Such defects and wrinkles on graphene skeleton are favorable for the nucleation of crystal seeds by self-assembly. Then the 'oriented attachment' can guide the nanoparticles' oriented growth. The oriented attachment mechanism describes self-organization of adjacent particles, so that they share a common crystallographic orientation, followed by joining of the particles at a planar interface. The process is particularly relevant in nanocrystalline regime, where bonding between particles reduces overall energy by removing surface energy associated with unsatisfied bonds [89].

3.2 PCMs/3D graphene foam as supercapacitor electrode

Till date, different kinds of nanostructured PCMs were deposited on the GF electrodes for supercapacitive application. So, we have categorized PCMs/GF electrodes for supercapacitors in three parts, such as metal oxide/GF, metal hydroxides/GF and conducting polymers/GF.

a) Metal oxides/3D graphene foam

Many transition metal oxides including RuO_2, MnO_2, NiO, Co_3O_4, CoO, etc. [90-94], are being investigated as one kind of PCMs for supercapacitors. However, most of the transition metal oxide-based materials result in a compromise of rate capability and reversibility because they rely on faradic redox reactions and suffer from low conductivity [95]. Its low electrical conductivity and crystal shrinkage/expansion while cycling induce flaking off during charge–discharge process [96, 97]. In this regard, researchers generally adopt conductive scaffolds (e.g., CNT, GNS, and NF) or conductive coatings (e.g., metals, carbons, and conducting polymers) to improve the conductivity of whole electrode [95-97]. The porous nanostructure design and conductivity engineering (e.g., combination between PCMs and highly conductive backbones) can effectively improve utilization of active materials and result in higher capacitance. Usually it is accepted that, directly grown nanostructures on current collectors (binder free) possess better mechanical and structural stability compared to powders attached on substrate [98-100]. According to above considerations, many researchers prepared and reported different nanostructures such as, nanofibers, nanorods, nanoflakes, etc, of transition metal oxides on 3D porous GF as supercapacitive electrode.

Dong et al [101] reported a simple hydrothermal procedure for cobalt oxide (Co_3O_4) nanowires (with 200-300 nm) via in situ deposition on 3D GF grown by CVD method. Authors used Co_3O_4/GF composite as the monolithic freestanding electrode for supercapacitor application and enzymeless electrochemical detection of glucose. Authors

demonstrated that, Co_3O_4/GF is electrode capable of delivering high specific capacitance of ~1100 F g^{-1} at a current density of 10 A g^{-1} in 1M KOH electrolyte with excellent cycling stability. This specific capacitance reported for Co_3O_4/GF electrode is several times larger than that of previously reported rGO-Co_3O_4 composite electrodes. Zhu et al [102] reported other polymorph of self-assembled cobalt oxide (CoO) nanorod cluster on GF (CoO-3DG) and nickel foam through a facile hydrothermal method followed by heat treatment. The prepared CoO-3DG electrode (980 F g^{-1}) exhibits good electrochemical performance, compared with CoO nanorod clusters grown on Ni foam (680 Fg^{-1}), at 1 A g^{-1} in 6M KOH electrolyte with excellent cycling stability (103%) for 10,000 cycles. Similarly, Deng et al [103] synthesized CoO nanobundles (NB) decorated with 3D GF electrode (CoO NB@GF), in which CoO NB consisted of porous nanoflakes. The CoO NB@GF electrode was prepared by combination of CVD, hydrothermal method and thermal treatment. The CoO NB@GF electrode exhibits high specific capacitance (352 F g^{-1} at 1 A g^{-1}), excellent rate capability (>88% retention when current increase from 1 A g^{-1} to 10 A g^{-1}) and cycling stability (nearly no diminution over 1000 cycles at 10 A g^{-1}). Besides cobalt oxide, nickel oxide is also a credential electrode material in supercapacitor application. So, Cao et al [104] prepared NiO on 3D GF by potentiostatic electrodeposition method for supercapacitor application. The NiO/GF electrode exhibits a better specific capacitance of 816 F g^{-1} than NiO/NF (305 F g^{-1}) at 5 mV s^{-1} and good rate capability in 3M KOH aqueous solution. Also, Wang et al [105] reported a pulsed laser deposition process using ozone as an oxidant to grow NiO nanoparticles on 3D GF. The NiO/GF electrode displays a high specific capacitance (1225 F g^{-1} at 2 A g^{-1}) and superb rate capability (68% capacity retention at 100 A g^{-1}).

The cobalt oxide and nickel oxide are the best candidates as PCMs with very high specific capacitance. Moreover, it has been reported that, mixed metal oxide ($NiCo_2O_4$) demonstrates improved electrical conductivity along with electrochemical activity due to more affluent redox reactions, including contributions from both nickel and cobalt ions, than solitary nickel oxide or cobalt oxide. Many studies focused on the optimization of morphology and incorporating $NiCo_2O_4$ with conductive materials to obtain high specific capacitance. Subsequently, Wei et al [106] synthesized $NiCo_2O_4$ on GF (rGO foam) by a combination of hydrothermal reaction and freeze-drying. In the fabrication of rGO foam, PU-sponge pieces were immersed in 20 mL mixture solution of rGO, under microwave irradiation at 90 ^oC for 30 min (pressure:~8 Bar), in a single mode microwave reactor. After freeze-drying for 48 hours, solvent within material was completely removed, and rGO–PU sponges were achieved. Further, ultrathin $NiCo_2O_4$ nanosheets, with thickness of few nanometers, were

prepared on rGO foam by hydrothermal method. The $NiCo_2O_4$@GF nanosheets exhibited a high capacitance about 778 F g^{-1} at a current density of 1 A g^{-1}, and an excellent cycling performance extending to 10,000 cycles at a high current density of 10 A g^{-1} compared to previous reports for $NiCo_2O_4$-graphene composite. Likewise, Nguyen et al [107] developed a facile and efficient two-step method for decoration of graphene sheets and nickel cobalt oxide ($NiCo_2O_4$) nanoparticles on conducting NF. In synthesis process, GO was deposited by potentiostatic mode on NF, in which GO concentration, direct current voltage, and deposition time were 1.5 g L^{-1}, 0.5 V, and 10 min, respectively. Secondly, bimetallic (Ni, Co) hydroxide was electrodeposited (at -1.0 V vs SCE) for 10 min on the G/NF electrode in a 6 mM $Co(NO_3)_2.6H_2O$ and 3 mM $Ni(NO_3)_2.6H_2O$ aqueous solution at room temperature. Finally, sample was placed in a quartz tube and calcined at 300 °C for 2 h at a ramping rate of 1^0C min^{-1} to convert hydroxide to $NiCo_2O_4$. The prepared electrode exhibited an ultrahigh specific capacitance of 2260 and 1950 F g^{-1} in KOH electrolyte at current densities of 1 and 7.5 A g^{-1}, respectively, with excellent rate capability, and exceptional cycling stability (92.8%) for 10,000 cycles.

Among all metal oxides, manganese oxide appears to be the most promising material as supercapacitor electrode with the advantages of low cost, environmental friendliness, abundance in nature, rapid charging-discharging and wide operating potential window (~1 V in aqueous electrolyte). So, different polymorphs of manganese oxide (MnO_2 and Mn_3O_4) were investigated on GF for supercapacitor application. Dong et al [108] reported different microstructures including homogeneous reticular, crumpled flower-like, flower-like and nano-bush of nanotubes for MnO_2 on GF by hydrothermal method for supercapacitor application. The maximum specific capacitance value about 284 F g^{-1} was reported for nanotubes like structure of MnO_2/GF electrode in Na_2SO_4 electrolyte at current density of 0.2 A g^{-1}. Similarly, He et al [109] and Sun et al [110] reported fabrication of MnO_2 nanoflakes on 3D GF by electrodeposition and hydrothermal deposition method for supercapacitor application, with maximum capacitance about 465 F g^{-1} at 2 mV s^{-1} and 210 F g^{-1} at a constant discharge current density of 2.0 A g^{-1}, in Na_2SO_4 electrolyte, respectively. A 3D hydrogel of graphene and MnO_2 nanoparticles were prepared using two-step synthesis by Wu et al [111]. The maximum specific capacitance for MnO_2/rGO foam achieved to be 242 F g^{-1} at a current density of 1 A g^{-1}.

Generally, 1D structure of materials such as nanowires, nanotubes, and nanoribbons can provide a unique opportunity to engineer electrochemical devices with improved electronic and ionic conductivity as well as electrochemical and structural transformations. The 1D

nanostructured MnO_2 is expected to offer larger specific surface area and carrying better charge storage performance than their bulk counterparts. Such 1D nanostructures can effectively combine the contribution from both surface and bulk-redox reactions. Accordingly, our group demonstrated [112] facile preparation and effective utilization of 1D α-MnO_2 nanofibers on 3D interconnected GF as supercapacitor electrode. The direct synthesis of α-MnO_2 nanofibers on GF was successfully achieved by facile solution growth (SG) method. The α-MnO_2 nanofibers were synthesized on graphene surface by using $MnSO_4$ and ammonium persulfate as oxidant. The XRD and Raman spectra (shown in Figure 5 (a, b)) of GF and MnO_2/GF electrode confirms the formation of α phase of MnO_2 on graphene skelton. Also, the SEM images (Figure 5(c, d, e)) reveals the formation of aggregated bundles (size about 15–30 nm) of 1D α-MnO_2 nanofibers grown well over 20–25μm wide graphene skeletons. High magnification SEM images illustrates that the nanofiber bundles (15–30 nm) are from individual MnO_2 nanofibers with a size of about ~5–10 nm in diameter. The capacitive performance of α-MnO_2/GF and α-MnO_2/CC (current collector) electrodes were tested in 1M Na_2SO_4 electrolyte. The cyclic voltammetry (CV) response of GF, α-MnO_2/CC and α-MnO_2/GF composite at 50 mV s^{-1} scan rate within 0 to 1 V potential window is shown in Figure 5(f). The CV curve shows less current density under curve for GF as compared to α-MnO_2/CC; however, α-MnO_2/GF shows higher current density under curve than α-MnO_2/CC. It indicates the increase in capacitive performance of α-MnO_2 nanofibers on GF. Such an increase in current under curve ascends mostly due to high surface area and interconnection between structural design provided by GF to α-MnO_2 nanofibers. The Figure 5(g) shows CV curves of α-MnO_2/GF at a different scan rate from 10 to 125 mV s^{-1}. It reveals rectangular shape of the CV curves maintained even at high scan rate, indicating good capacitive behavior with rapid diffusion and transportation of electrolyte ions from solution to pores of electrode materials representing good rate property. The calculated specific capacitance (see Figure 5(h)) for α-MnO_2/GF (670 F g^{-1}) is higher than that of α-MnO_2/CC (440 F g^{-1}) electrode at lowest scan rate 10 mV s^{-1}. Enhanced supercapacitive performance emanates from synergistic cooperation between GF and 1D α-MnO_2 nanofibers, which leads to maximum specific capacitance than conventional electrode architecture.

In summary of capacitive performances for various metal oxides/GF electrode (given in Table 1), bimetallic $NiCo_2O_4$ on GF electrodes prepared by Nguyen et al [107] achieves maximum specific capacitance around 2260 F g^{-1}. The maximum specific capacitance was obtained due to excellent interconnection between nanostructure (microflake) and graphene

by electrodeposition, and bimetallic oxides exhibits attractive redox properties than solitary metal oxide. However, $NiCo_2O_4$ on GF electrodes has limited operating potential window (-0.1 to 0.5 V) in aqueous electrolyte. Alternatively, with wide potential window 0 to 1.0 V (in aqueous electrolyte), MnO_2 nanofibers on GF achieves high capacitance ~670 F g^{-1} [112]. The 1D MnO_2 nanofibers synergistically with GF enhances the capacitance. Both these electrodes achieve maximum capacitance and wide potential window, which are imperative in respective of supercapacitor device applications.

b) Metal hydroxide/3D graphene foam

Besides the transition metal oxides, its hydroxides forms are also investigated as supercpacitor electrode such as $Ni(OH)_2$, $Co(OH)_2$, $NiCo(OH)_2$, $Cu(OH)_2$, etc, [113-116]. These metal hydroxides are advantageous in terms of fabrication using simple synthetic approaches (chemical methods), hydrous nature of material i.e. presence of structural water in the lattice, which provides nanostructured percolation pathways for proton conduction into the bulk of material. Also, hydrotalcite-like crystal structure of metal hydroxides consist of $M(OH)_{2-x}$ stacked layers intercalated with various anions (e.g., nitrate, carbonate, hydrate etc.) in the interlayer space to restore charge neutrality, can result higher electrochemical activity [117].

Among many metal hydroxides, $Co(OH)_2$ and $Ni(OH)_2$ with different polymorphs (α, β and γ) are the best candidates as a pseudocapacitive electrode material with very high specific capacitances, owing to their layered structures with large interlayer spacing and characteristic redox properties. For the first time, nanoporous nickel hydroxide [$Ni(OH)_2$] was grown by Ji et al [118] on surface of ultrathin-GF (UGF) via hydrothermal reaction. Nanoflakes like structure of $Ni(OH)_2$ were successfully grown on UGF using nickel chloride hexahydrate and urea as initial ingredient. In supercapacitive performance, gravimetric capacitance achieved ~1.56 X 10^3 F g^{-1} based on the mass of $Ni(OH)_2$ alone at 0.5 A g^{-1} current density in 6 M KOH aqueous solution. Furthermore, our group synthesized microflakes of $Ni(OH)_2$ on 3D GF by chemical method, using nickel chloride and ammonia as precursor and complexing agent, respectively. SEM images reveal (Fig. 6(a, b, c)) that, twigs of GF has been well covered with $Ni(OH)_2$ microflakes and magnified SEM images shows these flakes are 5-10 μm in width and 10-20 nm thick. Figure 6(d) shows CV curves of $Ni(OH)_2$/SS (stainless steel) and $Ni(OH)_2$/GF electrodes at 25 mV s^{-1}scan rate in 1M aqueous KOH electrolyte. The CV curves at different scan rates (25 to 100 mV s^{-1}) for $Ni(OH)_2$/GF electrode shown in

Figure 6(e). The maximum specific capacitance about 1,586 F g^{-1} and 655 F g^{-1} were obtained for $Ni(OH)_2$/GF and $Ni(OH)_2$/SS, respectively (Figure 6(f)). The improved synergistic interaction of graphene and $Ni(OH)_2$ ensures a superior electrode compared (~three times higher specific capacitance) to $Ni(OH)_2$ on SS. Recently, $Ni(OH)_2$ nanosheet/3D GF framework has been prepared by Ma et al [119] using CVD and hydrothermal method. The obtained $Ni(OH)_2$ nanosheet/3DGF electrode exhibits superior specific capacitance and rate capability than $Ni(OH)_2$/Ni foam and $Ni(OH)_2$ nanosheet/carbonfiber cloth electrodes. The $Ni(OH)_2$ nanosheet/3D GF electrode achieves an electrochemical capacitance as high as 2860 F g^{-1} at a current density of 2 A g^{-1}, and maintains 1791 F g^{-1} at 30 A g^{-1}.

Like $Ni(OH)_2$, cobalt hydroxide ($Co(OH)_2$) is also one of the best candidates as PCM due to its high theoretical specific capacitance, low cost and well-defined electrochemical redox activity. So, different morphologies of $Co(OH)_2$ on GF were prepared by our group using chemical bath deposition (CBD) [120] and potentiodynamic electrochemical deposition (PED) method [121]. The $Co(OH)_2$ nanorods, ~160-180 nm in diameter with needle like tip (SEM and TEM images are shown in Figure 7(a, b, c)), were prepared by CBD method using cobalt nitrate and urea as precursors. Figure 7(d, e) shows CV and galvanostatic charge-discharge curves at different scan rates (ranging from 25 to 125 mV s^{-1}) and charging current densities (from 5 to 15 A g^{-1}), respectively, for $Co(OH)_2$/GF electrode in aqueous 1M KOH solution. Maximum specific capacitances of (shown in Figure 7(f)) 1139 and 616 F g^{-1} were observed for $Co(OH)_2$/GF and $Co(OH)_2$/SS electrodes, respectively, at 10 A g^{-1} current density. Similarly, controlled flakes like $Co(OH)_2$ (see Figure 7(g, h, i)) were grown by PED method on GF. The CV curves in Figure 7(j) shows, that the current under curve of CV is higher for $Co(OH)_2$/MGF electrode than for $Co(OH)_2$/SS and MGF electrode. This results confirms that $Co(OH)_2$/MGF electrode shows more storage capacity than $Co(OH)_2$/SS and MGF electrodes. The GCD graphs of $Co(OH)_2$/MGF at different current densities from 9.09 to 45.5 A g^{-1} and calculated specific capacitance shown in Figure 7(k, l) demonstrate high specific capacitance about (~1030 F g^{-1}).

The mixed metal hydroxides (MMH) containing transition metals have also been investigated as active electrode materials for supercapacitors. A general chemical formula of $[M^{2+}_{1-x}M^{3+}_{x}(OH)_2].mH_2O$ is used to present MMH materials which have an attractive redox property, and most of their growth techniques are environmentally friendly. Since, MMH materials like CoNi and NiAl MMH on GF were prepared using chemical methods for supercapacitor application by our group [122], Dong et al [123] and Momodu et al [124],

respectively. The nanostructured $Co_xNi_{1-x}(OH)_2$ films with different Ni:Co (x=0.33, 0.5, 0.66 and 1) compositions on GF are prepared by using CBD method. The CBD method comprises, heating the bath consist of GF in equimolar metal salts (cobalt nitrate and nickel nitrate) and urea at 120 °C for 4h. The $Co_xNi_{1-x}(OH)_2$ demonstrates composition-dependent microstructures with randomly grown nanorod-like morphology. The SEM analysis (shown in Figure 8(a-e)) reveals that, nanorods of $Co(OH)_2$ reduce in size from 180 to 35 nm with increases in nickel content and are converted into the $Ni(OH)_2$ fuzzy nanoparticle structure. Typical CV curves of electrode for different x (Ni) values (x= 0 to 1) are shown in Figure 8(f), and all curves display two prominent characteristic redox peaks, which specify pseudocapacitive behaviour of electrode. The CV curves shows shift in redox peaks with compositions of the $Co_xNi_{1-x}(OH)_2$. Figure 8(g) shows GCD plots of $Co_xNi_{1-x}(OH)_2$/GF within potential window of 0 to 0.5 V at a constant charging current of 60 A g^{-1}. The graph of specific capacitance with different Ni:Co compositions (shown in Figure 8(h)) reveals that solitary $Co(OH)_2$/GF shows higher capacitance than that of solitary $Ni(OH)_2$/GF, and combined supercapacitance of $Co_{0.66}Ni_{0.33}(OH)_2$/GF (1280 F g^{-1}) is higher than that of individual $Ni(OH)_2$/GF and $Co(OH)_2$/GF. Further, optimised electrode was tested for supercapacitive performance and it exhibits maximal specific capacitance ~1847 F g^{-1} at 5 A g^{-1}. Similarly, new type of 3D GF nanohybrid electrode based on microscopic GF loaded nickel-cobalt hydroxides nanoflakes ($Ni_xCo_{2x}(OH)_{6x}$/GF) synthesized by Dong et al [123] using one-step electrochemical method for supercapacitor application. In the GF fabrication, nickel foam was soaked in GO solution (4 mg mL^{-1}), then reduced it using electrochemical method in 0.1 M Na_2SO_4 within potential window -0.2 to -1.5 V (vs SCE) at 50 mV s^{-1} scan rate, product was denoted as rGOF. The one-step electrochemical synthesis of $Ni_xCo_{2x}(OH)_{6x}$/rGOF was carried out in 0.1 M Na_2SO_4 aqueous solution containing 20 mM $NiSO_4$ and 20 mM $CoSO_4$ in potential range from -0.2 to -1.5 V at 50 mV s^{-1} scan rate. Authors found that, the specific capacitance of $Ni_xCo_{2x}(OH)_{6x}$ nanoflakes on bare Ni foam is much lower than those deposited on rGOF support (703 F g^{-1}). Momudu et al [124] demonstrated excellent pseudocapacitive behaviour of nickel-aluminum double hydroxide microspheres (Ni-Al DHM) synthesized by a facile solvothermal technique using tertabutanol as structure-directing agent on nickel foam-graphene (NF-G by CVD method) current collector as compared to bare nickel foam. The Ni-Al DHM with NF-G current collector exhibits an enhanced supercapacitive performance due to the presence of conductive graphene layer on the nickel foam and gives a specific capacitance of 1252 F g^{-1} at a current density of 1 A g^{-1} with a capacitive stability of about 97% after 1000 cycles.

So far, capacitive performances (shown in table 2) of metal hydroxides on GF, the $Ni(OH)_2$ nanosheets prepared by Ma et al [119] using facile hydrothermal method on GF achieves maximum specific capacitance about 2860 F g^{-1} with 65% stability over 1000 cycles. The hierarchical porous structure of $Ni(OH)_2$ nanosheets as building blocks, which is assembled tightly on matrix of 3D graphene, contribute to achieve maximum specific capacitance.

c) Conducting polymers/3D graphene foam

Conducting polymers such as polyaniline, polypyrrole and PEDOT have been recognized as PCMs due to their high accessible surface area, low resistance, high stability and other fascinating properties. Conducting polymers are promisingly useful to composite with graphene or graphene derived materials to achieve high-performance for 3D GF-based supercapacitor electrodes. Many of researchers explored graphene-PANI composite based on inter-stacked reduced graphene oxides (rGOs) [125, 126]. Primarily, Tai et al [127] reported polyaniline/GF (PANi/GF) composite hydrogel as supercapacitor electrode prepared via a self-assembled method followed by in situ polymerization of aniline. The PANi/GF composite hydrogel at room temperature exhibits largest specific capacitance of 334 F g^{-1}, which is about 150% higher than that of pure GNS hydrogel at 2 A g^{-1} in 6M KOH electrolyte. Furthermore, Dong et al [128] reported a free-standing and flexible supercapacitor electrode based on PANI/GF hybrid, exhibit specific capacitances 346 F g^{-1} at 4 A g^{-1} current density in 1M H_2SO_4. PANI was grown by in-situ polymerization of aniline monomers in HCl acidic media with ammonium peroxydisulfate (APS) oxidant on 3D GF at room temperature. Specific capacitance was increased as compared to the report by Wang et al [129] for graphene-PANI composite 233 F g^{-1} using 2D graphene. Liu et al [130] synthesized polyaniline/GF 3D nanocomposite as supercapacitor electrode via in-situ polymerization of aniline monomer on graphene surface. The observed gravimetric capacitance at low scan rate of 1 mV s^{-1} is 463 F g^{-1} in 3M KOH basic aqueous electrolyte. Chen et al [131] fabricated 3D porous graphene-based polyaniline composite as electrode material. Polyaniline was homogeneously coated on 3D graphene (ERGO) porous material prepared by electrochemical reduction of concentrated graphene oxide. ERGO–polyaniline composite electrode has shown specific capacitance about 716 F g^{-1} at 0.47 A g^{-1}.

Our group [132] reported chemical homogeneous growth of polyaniline nanofibers (SEM images shown in Figure 9(a, b, c)) on porous GF as supercapacitor electrode material. The XRD pattern shown in Figure 9(d) and photograph of PANI/GF electrode shown in inset

reveal formation of green colored PANI with semi-crystalline nature. The comparative CV of PANI/SS and PANI/GF as electrode in aqueous 1M H_2SO_4 electrolyte at 50 mV s^{-1} scan rate within optimized voltage window of -0.15 to 0.8 V Vs Ag/AgCl are shown in Figure 9(e). The current under curve is significantly higher for PANI/GF than for PANI/SS electrode, recommends supremacy of PANI/GF for supercapacitor application. Comparative GCD plots of PANI/SS and PANI/GF within potential range of -0.15 to 0.8 V at constant charging current of 1 mA cm^{-2} are shown in Figure 9(f). The comparative examination of GCD curves points out resistive drop (iR) of PANI/SS (~0.447 V) is substantial than that of PANI/GF (~0.066 V) electrode. PANI/GF electrode shows approximately more than ~7 times less iR drop, reveling more proficiency as supercapacitor electrode material. Obviously, the impeccably interconnected 3D GF offers much better conduction pathways for charge transportation. Also, to confirm good conductivity of GF based PANI electrode, Nyquist plots of PANI/SS and PANI/GF electrodes are compared in Figure 9(g). A sharp increase of Z_{im} at lower frequency attributed to capacitive behavior of material, however, semi-circle at higher frequencies implies charge transfer resistance (R_{ct}) at electrode/electrolyte interface. Apparently, PANI/GF electrode preserves a much lower resistance than PANI/SS electrode (~10 and ~70 Ω). This explores that the GF based PANI electrode possesses lower contact and charge-transfer impedances. Inset of Figure 9(g) showed Ragone plot regarding energy and power densities with current densities of 1 to 4 mA cm^{-2}. The specific power (SP), specific energy (SE) for PANI/GF at 1 mA cm^{-2} is found to be ~3 kW kg^{-1}, ~120 Wh kg^{-1}, respectively. The columbic efficiency of nanofibers PANI/3D GF electrode at different current densities is plotted in inset of Ragone plot. The maximal specific capacitance of PANI/GF electrode was found to be 1024 F g^{-1} in 1 M H_2SO_4 at 10 mV s^{-1} scan rate (1002 F g^{-1} at 1 mA cm^{-2} discharge current density).

Zhang et al [133] prepared polyaniline-filled GF as supercapacitor electrode with large areal capacitance of 1700 mF cm^{-2}. Mesoporous polyaniline was deposited over macroporous GF with different deposition time via incorporation of electrodeposition and inkjet techniques. Alongside with PANI, Polypyrrole is also well-known PCM for supercapcitors. Zhang et al [134] designed graphene–hollow polypyrrole (PPy) nanoarchitecture electrode material, wherein hollow PPy spheres incorporated in between graphene layers. This is assembled by mixing graphene oxide and polystyrene(PS)@PPy core–shell sphere, followed by successive graphene oxide reduction and PS etching. The graphene–hollow PPy nano-architecture electrode shown 500 F g^{-1} specific capacitance at current density of 5 A g^{-1}.

In development of conducting polymers/GF 3D electrodes (comparative capacitive performance tabulated in Table 3), PANI prepared by our group [132] displays better supercapacitive performance in terms of specific capacitance ~1024 F g^{-1} with good stability over 5000 cycles. The increased specific capacitance, good cycling stability and improved capability of the PANI/GF 3D electrode can be attributed to active PANI nanofibers with a large specific surface area and the unique structure of the graphene backbone offering efficient conducting pathways. All these important aspects promote the effectiveness of the 3D graphene framework serving as a multifarious booster for superior electrochemical performance of PANI.

3.3 PCMs/Carbon nanotubes/3D graphene foam

The seamlessly continuous 3D graphene with an excellent high specific surface area due to the strong π–π interaction between graphene sheets and porous structure, which are suitable to make functional composites by surface modification with other functional materials or carbon based materials. Furthermore, surface area of 3D GF can be enhancing by reducing the pore size (few hundred micrometres) via filling macroporous structure that limits boosting the performance of supercapcitors. The shortcoming of surface area can be overcome by combination of graphene and carbon nanotube, it can enhance effective surface area with their axial (1D) geometry. Theoretical calculation has indicated that covalently bonded graphene and carbon nanotubes could lead to superior properties (surface area, mechanical strength etc.,) in three dimensions while maintaining inherited properties in planar and axial directions [135]. Compared with their single components, hybrid structures such as CNTs/graphene shown improved physical and chemical properties, including enhanced electric and thermal conductivity, mechanical flexibility, due to synergistic effects. In addition, the surface roughness of CNTs/graphene is beneficial for fabrication of PCMs-graphene based composites.

So, there are few attempts made to prepare high quality CNT/graphene hybrid foam electrodes for supercapacitors, including chemical methods [136-140] and chemical vapor deposition [141-148]. Cheng et al [136] prepared graphene/SWNTs composite for EDLC based capacitors by blending process. To fabricate composite material, CVD prepared SWCNTs were ultrasonicated in GO suspension (mass ratio of CNT/GO is 1:10) for different time. Similarly, the 3D N-doped Graphene/CNT hybrid foams were prepared by You et al [137] via simple liquid phase hydrothermal treatment followed by freeze-drying with

carbonization of graphene oxide dispersed pristine CNTs in presence of pyrrole. Also, a novel method was reported by Beidaghi et al [138] for fabricating micro-patterned interdigitated of rGO/CNTs composites by combining electrostatic spray deposition (ESD) and photolithography lift-off methods for ultra-high power handling micro-supercapacitor application. Considering the low EDLC capacitance (usually exhibited by carbon based materials), many researchers are loading psuedocapacitive materials on 3D CNTs/GF electrodes to enable its high specific capacitance [139, 140]. Moon et al [139] and Zhang et al [140] prepared MnO_x/CNT(COOH)/GF and Mn_2O_3/CNT/GF, respectively for high performance supercapacitive application. Moon et al prepared a MnO_x material on functionalized CNTs (COOH/CNT) by hydrothermal method in the presence of GF. Zheng et al deposited CNTs on CVD prepared GF by using electrodeposition method. Further, Mn_2O_3 was prepared by electrodeposition method on CNT/GF electrode at constant potential of 1.0 V in an aqueous solution of 0.01 mol L^{-1} manganese acetate for different deposition time. Mn_2O_3/CNTs/GF exhibits maximum specific capacitance of about 370 F g^{-1}.

However, relatively poor connection between graphene and CNTs in chemical synthesis limits its application in fast charge–discharge energy storage devices. Preparation of high-quality graphene/CNT hybrid materials with strong bonding, by in situ growth using CVD method, is a promising technique. Therefore, it is highly desirable to fabricate graphene/CNT hybrid films with strongly connected and large quantity of CNTs that could substantially extend the porous architecture and enlarge the surface area. Therefore, Fan et al [141], Yan et al [142] and few others [143-145] reported direct growth of CNTs on graphene and their application for EDLC based supercapacitors. It should be noted that, in above-mentioned studies CNTs are grown only on graphene surfaces, where the catalyst particles are deposited by e-beam evaporation, dip-coating or other methods. Initially, Du et al [146] developed a rational strategy for creating 3D pillared vertically aligned carbon nanotube (VACNT)-graphene architectures by intercalating growth of VACNTs (with controlled length) into thermally expanded highly ordered pyrolytic graphite (HOPG). Additionally, in conjunction with electrodeposition of nickel hydroxide ($Ni(OH)_2$) to introduce the pseudocapacitance, these 3D pillared VACNT graphene architectures with a controllable nanotube length were demonstrated a high specific capacitance (~1384 F g^{-1}) and remarkable rate capability (99% for 20,000 cycles). Moreover, Liu et al [147] prepared MnO_2/CNT/GF and PPy/CNT/GF electrodes for asymmetric supercapacitors. The MnO_2 nanosheets were grown on CNT/GF hybrid film using a hydrothermal method for supercapacitor application.

Zhu et al [148] synthesized MnO_2-CNT-graphene-Ni hybrid foams in which carbon nanotube (CNT)-graphene hybrids were grown on porous Ni foam, and used as substrates to immobilize MnO_2 nanoflakes (schematic shown in Figure 10 (a)). As-prepared hybrid materials were used as supercapacitor electrodes, which fully maintain high conductivity and high surface-to-volume ratio of CNTs, large pseudocapacitance of MnO_2 nanoflakes and high porosity provided by framework of Ni foam. The conductivity of the 3D MnO_2–CNT–graphene–Ni foam is as high as 117 S cm^{-1} due to seamless integration of MnO_2 nanoflakes, CNTs, graphene and Ni foam among the 3D frameworks, which guarantee its low internal resistance (1.25 ohm) when compacted into supercapacitor devices. Raman, XRD and SEM analysis (shown in Figure 10 (b, c, d)), confirm the formation of nanoflakes of MnO_2 over CNTs/GF. In electrochemical capacitive performance shown in Figure 10 (e, f), the 3D MnO_2/CNT/graphene/Ni based prototype supercapacitors show specific capacitances of ~251 F g^{-1} in aqueous electrolytes with good cycling stability of 82% for 3000 cycles (at a current density of 1.0 A g^{-1}). In addition, these 3D hybrids also demonstrate their potential in all-solid-state flexible supercapacitors.

In the capacitive performances of PCMs/CNT/GF electrode assemblies (listed in Table 4) for supercapcitor application, Du et al [146] achieved maximum specific capacitance of about 1384 F g^{-1} for $Ni(OH)_2$/CNT/GF electrodes. The observed excellent electrochemical performance of the $Ni(OH)_2$-coated CNT/graphene electrode could be attributed to their unique 3D porous structure. First, the vertically aligned CNT and graphene conductive network allows for efficient charge transport. Second, the inherently porous structure could significantly facilitate the electrolyte diffusion and, hence, an enhanced ionic conductivity.

3.4 Symmetric and asymmetric device performances

To meet ever-increasing energy and power demands, innovation of new materials along with fabrication of symmetric/asymmetric devices is an effective approach for supercapacitors. Conventionally two identical electrodes separated by electrolyte based device termed as symmetric supercapacitors and asymmetric capacitors consist of two dissimilar electrodes; often carbon and PCM based electrode (schematics are shown in the Figure 11(a)) [149]. The asymmetrical supercapacitor having higher power density is advantageous because of non-identical voltage changes in the two electrodes. However, asymmetric supercapacitors suffer from low value of specific energy. This difficulty can be inhibited through the fabrication of symmetric supercapacitors [150]. It is worth noting that, the cell voltage is depended on several factors including intrinsic electrochemical reactions,

electrolyte species, and macroscopic structure of cell. In view of that, many researchers fabricated symmetric and asymmetric devices based on PCMs/GF electrodes.

He et al [109] fabricated flexible supercapacitors in symmetric mode using both electrodes as MnO_2/GF with a polymer separator and two PET membranes, which showed 6.8 Wh kg^{-1} and 0.62 kW kg^{-1} energy and power density, respectively for potential window 0-1.0 V in 0.5 M Na_2SO_4. Wu et al [111] assembled asymmetric device with MnO_2/GF hydrogel as positive and pure rGO hydrogel as negative electrode, and achieved improvement in potential range 0-1.6 V with energy density 21.2 Wh kg^{-1} and power density 0.82 kW kg^{-1}. We achieved enhanced energy density 13.9 Wh kg^{-1} and power density 18 kW kg^{-1} with potential range 0-1.2 V at 5 A g^{-1} in KOH for symmetric $Co(OH)_2$/GF supercapacitive device [120]. Wang et al [105] reported asymmetric supercapacitive device using NiO/3D GF as positive and nitrogen-doped carbon nanotubes as negative electrode with energy and power density values 32 Wh kg^{-1} and 0.7 kW kg^{-1} respectively, with voltage window 0-1.4 V in 1M KOH. Ji et al [118] constructed asymmetric cell wherein $Ni(OH)_2$/UGF worked as positive electrode and activated microwave exfoliated graphite oxide acts as negative electrode with increase in energy and power density values 6.9 Wh kg^{-1} and 44 kW kg^{-1} in 6M KOH within wider potential window 0-1.8 V at 2 A g^{-1}.

Concerning the usage of environmental friendly aqueous electrolyte, PCMs/GF based supercapacitors shows their potential for application as high power and energy supercapcitor devices. To demonstrate practical application of PCM/GF based symmetric devices, we used it to run toy fan and glow LED (shown in Figure 11(b)). The Ragone plot is shown in Figure 11(c), which is summarizing the energy and power density of PCMs/GF based devices [105, 109, 111, 118, 120, 151, 152] with high-end commercial supercapacitor devices. The PCM/GF based hybrid supercapacitors have comparable or higher energy density than most of the organic-based high-end supercapacitors, but the power density is much higher (~20 times higher) than that of all cells available commercially. In Ragone plot, the supercapacitive performances of metal hydroxides on GF electrodes are superior to that of other PCMs/GF electrodes based devices (as shown in Figure 11 (c)).

4 Perspective, challenges and future directions

This feature article provides a brief description of diverse synthetic approaches that can be used for preparation graphene-based 3D architectures and its composites with PCMs. In these, 3D GF based materials for supercapacitors, emphasis is given to synergistic effects between 3D graphene and PCMs. The GF can serve as an ideal 3D support for growing or

assembling nanomaterials with well-defined structures. Based on the outcomes, superiority of 3D GF electrodes over conventional electrodes such as metal current collector (MCC), graphene paper, NF etc., is discussed in brief.

1) *Porous and freestanding structure:* In most of the works on graphene-based composites, PCMs nanostructures are incorporated as guests onto 2D GNS, and those structures usually suffer from serious aggregation, which would cause inferior accessibility of electrolyte ions to active material surface. The aggregation of GNS hinders the rapid electrolyte diffusion and reduces the surface area, and consequently decreases the performance of electrodes. The freestanding 3D interconnected structure of GF is efficient solution for aggregation. Usually, in supercapacitors, large surface area and fast electrolyte transport near electrode surface are required in order to obtain high rate of electrochemical reaction. So, macro-porous structure of GF is advantageous in terms intercalation of electrolyte through the bulk of electrode.
2) *Lightweight:* In order to evaluate supercapcitor performance, the specific capacitance (F g^{-1}), energy density (Wh kg^{-1}) and power density (W kg^{-1}) are the most important parameters. Therefore, weight of electrode materials is a very significant feature, particularly in portable electronic devices. Currently, in commercial supercapacitors, weight of conductive substrates (NF or MCC) accounts for a large mass portion in the device, but these conductive substrates do not contribute to the capacitance and translates to an effectively lower energy density and power density. Hence, lightweight GF are beneficial for supercapacitor devices.
3) *Interconnected 3D structure and electrical conductivity:* Generally, conventional architecture (PCMs on MCC or carbon paper and PCMs-GO composites with surface-anchored, layer-by-layer assembled and randomly mixed architectures) offer self-dimensional restrictions in charge transportation during charge-discharge process. Enriched resistive binder, loosely interconnected nanostructures or contact resistance between GO-PCMs (at high thickness) restrict easy charge transportation towards the MCC (schematic of charge transport mechanism is shown in Figure 12(a)). However, 3D GF serves high surface area with easy charge transportation during charge-discharge process. As current collector, GF with porous 3D interconnected structure improves the electronic and ionic conductivity of PCMs nanostructure by providing a low diffusion path.
4) *Structural stability:* In order to fulfil long cycling life (more than 10^4 times), the electrode materials must have strong structural stability. Generally, it is accepted that,

the electrode with porous structure and feasible charge transportation can sustain for longer cyclic stability.

Despite many advantages offered by 3D GF, some challenges in fabrication processes and supercapacitor application still exist. We would like to mention that the inherent properties of these materials need to be explored and should be overcome.

1) Different fabrication process provides some advantages and drawbacks. Compared to traditional 3D GF assembled by GNS, the GF synthesized by CVD with NF as template, presents some peculiar advantages such as high conductivity (less inter-sheet junction resistance) and specific surface area (strong π-π interaction). However, GF assembled by GNS provides more nucleation sites to the growth of PCM nanostructures. In future, researchers likely to focus on controlling GO distribution, density, chemical bonding, as well as 3D arrangement with enhancing mechanical strength of GF.
2) The surface area of 3D GF is limited due to its macroporous structure with pore sizes of few hundred micrometers. So, many researchers are focusing on the combination of 3D GF and carbon nanotube or other conductive materials, to overcome the shortage of limited effective surface area due to their planar (2D) geometry (schematic is shown in Figure 12(b)), and the roughness surface of CNTs/graphene is convenient for further growth of PCMs based composites. Recent research focus is gaining much attention on how to increase the surface area of GF by reducing or controlling the pore structure via loading other conducting materials.

In summary, various types of PCMs on GF electrodes offer different advantages and suffer from some inadequacies in supercapcitor application. Such as, metal hydroxide reveals maximum capacitance ($Ni(OH)_2$-2860 F g^{-1}) but fails to achieve decent operating potential window (~0.6 V in aqueous electrolyte) and cyclic stability (65% for 1000 cycles) [119]. Conversely, in metal oxides/GF exhibits excellent cyclic stability ($NiCo_2O_4$-93%, 10,000 cycles), but, could not achieve high specific capacitance (2860 F g^{-1}) compare to its hydroxides counterpart [107]. On the other hand, conducting polymers/GF exhibits decent specific capacitance (PANI-1024 F g^{-1}) with wide potential widow (~1 V) but it suffers from less cyclic stability (86%, 5000 cycles) [132]. These different kinds of PCMs/GF electrodes can be used in various imperative supercapcitor devices, where high capacitance or voltage requires. However, the supercapacitve performances, in terms of power and energy density, metal hydroxides on GF electrodes are superior and compatible for devices compared to other

PCMs/GF electrodes (see Figure 11 (c)). In conclusion, we consider that the study of hierarchical composites based on 3D GF and PCMs, is still in its infancy despite the numerous works mentioned in this feature article. The exponential growth of publications in this field observed in recent years is most likely due to outstanding potential of 3D GF for supercapacitors. In recent times, many researchers are devoting ever-increasing efforts to the search of 3D GF related functional materials for supercapacitor application. We are strongly convinced that those novel 3D GF based materials would bring more exciting results in future as working electrodes for next generation supercapacitors.

Acknowledgment

This work was partially supported by the Yonsei University Research Fund of 2013, the Pioneer Research Center Program (2010-0019313), the Priority Research Centers Program (2009- 0093823), the Basic Science Research Program (2012-8-0622) through the National Research Foundation (NRF) of Korea funded by the Ministry of Science, ICT & Future Planning and Korea Electric Power Corporation Research Institute though Korea Electrical Engineering & Science Research Institute. [Grant number: R14XA02-2]

References

1. G. Wang, L. Zhang and J. Zhang, *Chem. Soc. Rev.*, 2012, **41**, 797-828.
2. A. F. Burke, *Proc. IEEE*, 2007, **95**, 806-820.
3. M. Winter and R. J. Brodd, *Chem. Rev.*, 2004, **104**, 4245-4270.
4. H. Pan, J. Li and Y. P. Feng, *Nanoscale Res. Lett.*, 2010, **5**, 654-668.
5. R. A. Fisher, M. R. Watt and W. J. Ready, *ECS J. Solid State Sci. Technol.*, 2013, **2**, M3170-M3177.
6. V. V. Obreja, *Physica E: Low-dimens. syst. Nanostruct.*, 2008, **40**, 2596-2605.
7. E. Frackowiak and F. Beguin, *Carbon*, 2001, **39**, 937-950.
8. F. Markoulidis, C. Lei, C. Lekakou, E. Figgemeier, D. Duff, S. Khalil, B. Martorana and I. Cannavaro, *IOP Conference Series: Materials Science and Engineering*, 2012, **40**, 012021.
9. D. Saha, Y. Li, Z. Bi, J. Chen, J. K. Keum, D. K. Hensley, H. A. Grappe, H. M. Meyer, S. Dai, M. P. Paranthaman and A. K. Naskar, *Langmuir*, 2014, **30**, 900-910.
10. C. Liang, Z. Li and S. Dai, *Angew. Chem. Int. Ed.*, 2008, **47**, 3696-3717.
11. D. Sun, X. Yan, J. Lang and Q. Xue, *J. Power Sources*, 2013, **222**, 52-58.
12. M. D. Stoller, S. Park, Y. Zhu, J. An and R. S. Ruoff, *Nano Lett.*, 2008, **8**, 3498-3502.
13. X.-Y. Peng, X.-X. Liu, D. Diamond and K. T. Lau, *Carbon*, 2011, **49**, 3488-3496.
14. J. Zang, C. Cao, Y. Feng, J. Liu and X. Zhao, *Sci. Rep.*, 2014, **4**, 6492.
15. P. Simon and Y. Gogotsi, *Nat. Mater.*, 2008, **7**, 845-854.
16. V. Singh, D. Joung, L. Zhai, S. Das, S. I. Khondaker and S. Seal, *Prog. Mater Sci.*, 2011, **56**, 1178-1271.
17. H.-J. Choi, S.-M. Jung, J.-M. Seo, D. W. Chang, L. Dai and J.-B. Baek, *Nano Energy*, 2012, **1**, 534-551.
18. L. Grande, V. T. Chundi, D. Wei, C. Bower, P. Andrew and T. Ryhänen, *Particuology*, 2012, **10**, 1-8.
19. D. A. Brownson, D. K. Kampouris and C. E. Banks, *J. Power Sources*, 2011, **196**, 4873-4885.
20. A. K. Geim and K. S. Novoselov, *Nat. Mater.*, 2007, **6**, 183-191.
21. A. K. Geim, *Science*, 2009, **324**, 1530-1534.
22. A. H. Castro Neto, F. Guinea, N. M. R. Peres, K. S. Novoselov and A. K. Geim, *Rev. Mod. Phys.*, 2009, **81**, 109-162.
23. J. Kim, J. Oh, C. In, Y.-S. Lee, T. B. Norris, S. C. Jun, and H. Choi, *ACS Nano*, 2014, **8**, 2486-2494.

24. K. Choi, J. Lim, J. R. Rani, H. S. Yoon, J. Oh, T. Hong, T. Ha, B. C. Park, K. I. Sim, S. C. Jun, and J. H. Kim, *Appl. phys. Lett.*, 2013, **102**, 131901-1-4.
25. H. Park, H. S. Yoon, U. Patil, R. Anoop, J. Lee, J. Lim, W. Lee, S. C. Jun, *Biosens. Bioelectron.*, 2014, **54**, 141-145.
26. C. Liu, Z. Yu, D. Neff, A. Zhamu and B. Z. Jang, *Nano Lett.*, 2010, **10**, 4863-4868.
27. Q. Lu, J. G. Chen and J. Q. Xiao, *Angew. Chem. Int. Ed.*, 2013, **52**, 1882-1889.
28. M. Jayalakshmi and K. Balasubramanian, *Int. J. Electrochem. Sci*, 2008, **3**, 1196-1217.
29. H. Ibrahim, A. Ilinca and J. Perron, *Renew. Sust. Energ. Rev.*, 2008, **12**, 1221-1250.
30. X. Lang, A. Hirata, T. Fujita and M. Chen, *Nat. Nanotechnol.*, 2011, **6**, 232-236.
31. X. Xia, J. Tu, Y. Zhang, X. Wang, C. Gu, X.-b. Zhao and H. J. Fan, *ACS nano*, 2012, **6**, 5531-5538.
32. Y.-B. He, G.-R. Li, Z.-L. Wang, C.-Y. Su and Y.-X. Tong, *Energy Environ. Sci.*, 2011, **4**, 1288-1292.
33. H. Jiang, T. Zhao, C. Li and J. Ma, *J. Mater. Chem.*, 2011, **21**, 3818-3823.
34. V. Gupta, S. Gupta and N. Miura, *J. Power Sources*, 2008, **175**, 680-685.
35. M. Mastragostino, C. Arbizzani and F. Soavi, *Solid State Ionics*, 2002, **148**, 493-498.
36. M. E. Roberts, D. R. Wheeler, B. B. McKenzie and B. C. Bunker, *J. Mater. Chem.*, 2009, **19**, 6977-6979.
37. G. A. Snook, P. Kao and A. S. Best, *J. Power Sources*, 2011, **196**, 1-12.
38. M. Zhi, C. Xiang, J. Li, M. Li and N. Wu, *Nanoscale*, 2013, **5**, 72-88.
39. Q. Cheng, J. Tang, J. Ma, H. Zhang, N. Shinya and L.-C. Qin, *Carbon*, 2011, **49**, 2917-2925.
40. S. Chen, J. Zhu, X. Wu, Q. Han and X. Wang, *ACS nano*, 2010, **4**, 2822-2830.
41. L. L. Zhang, R. Zhou and X. Zhao, *J. Mater. Chem.*, 2010, **20**, 5983-5992.
42. H. Wang, Q. Hao, X. Yang, L. Lu and X. Wang, *Electrochem. Commun.*, 2009, **11**, 1158-1161.
43. B. Zhao, J. Song, P. Liu, W. Xu, T. Fang, Z. Jiao, H. Zhang and Y. Jiang, *J. Mater. Chem.*, 2011, **21**, 18792-18798.
44. H. Wang, H. S. Casalongue, Y. Liang and H. Dai, *J. Am. Chem. Soc.*, 2010, **132**, 7472-7477.
45. C. Nethravathi, M. Rajamathi, N. Ravishankar, L. Basit and C. Felser, *Carbon*, 2010, **48**, 4343-4350.
46. K. Zhang, L. L. Zhang, X. Zhao and J. Wu, *Chem. Mater.*, 2010, **22**, 1392-1401.

47. D. Zhang, X. Zhang, Y. Chen, P. Yu, C. Wang and Y. Ma, *J. Power Sources*, 2011, **196**, 5990-5996.
48. W. Wang, S. Guo, M. Penchev, I. Ruiz, K. N. Bozhilov, D. Yan, M. Ozkan and C. S. Ozkan, *Nano Energy*, 2013, **2**, 294-303.
49. H. Ji, L. Zhang, M. T. Pettes, H. Li, S. Chen, L. Shi, R. Piner and R. S. Ruoff, *Nano Lett.*, 2012, **12**, 2446-2451.
50. T. Maiyalagan, X. Dong, P. Chen and X. Wang, *J. Mater. Chem.*, 2012, **22**, 5286-5290.
51. Y. Xue, J. Liu, H. Chen, R. Wang, D. Li, J. Qu and L. Dai, *Angew. Chem. Int. Ed.*, 2012, **51**, 12124-12127.
52. F. Yavari, Z. Chen, A. V. Thomas, W. Ren, H.-M. Cheng and N. Koratkar, *Sci. Rep.*, 2011, **1**, 166, 1-5.
53. X. Dong, X. Wang, L. Wang, H. Song, H. Zhang, W. Huang and P. Chen, *ACS Appl. Mater. Interfaces*, 2012, **4**, 3129-3133.
54. M. T. Pettes, H. Ji, R. S. Ruoff and L. Shi, *Nano Lett.*, 2012, **12**, 2959-2964.
55. X. Dong, J. Chen, Y. Ma, J. Wang, M. B. Chan-Park, X. Liu, L. Wang, W. Huang and P. Chen, *Chem. Commun.*, 2012, **48**, 10660-10662.
56. H. Bi, X. Xie, K. Yin, Y. Zhou, S. Wan, L. He, F. Xu, F. Banhart, L. Sun and R. S. Ruoff, *Adv. Funct. Mater.*, 2012, **22**, 4421-4425.
57. K. S. Novoselov, A. K. Geim, S. V. Morozov, D. Jiang, Y. Zhang, S. V. Dubonos, I. V. Grigorieva and A. A. Firsov, *Science*, 2004, **306**, 666-669.
58. S. He and W. Chen, *Nanoscale*, 2015, DOI: 10.1039/c1034nr05895j.
59. M. J. Allen, V. C. Tung and R. B. Kaner, *Chem. Rev.*, 2009, **110**, 132-145.
60. C. Berger, Z. Song, X. Li, X. Wu, N. Brown, C. Naud, D. Mayou, T. Li, J. Hass and A. N. Marchenkov, *Science*, 2006, **312**, 1191-1196.
61. K. S. Kim, Y. Zhao, H. Jang, S. Y. Lee, J. M. Kim, K. S. Kim, J.-H. Ahn, P. Kim, J.-Y. Choi and B. H. Hong, *Nature*, 2009, **457**, 706-710.
62. S. Park and R. S. Ruoff, *Nat. Nanotechnol.*, 2009, **4**, 217-224.
63. Y. Hernandez, V. Nicolosi, M. Lotya, F. M. Blighe, Z. Sun, S. De, I. McGovern, B. Holland, M. Byrne and Y. K. Gun'Ko, *Nat. Nanotechnol.*, 2008, **3**, 563-568.
64. N. Behabtu, J. R. Lomeda, M. J. Green, A. L. Higginbotham, A. Sinitskii, D. V. Kosynkin, D. Tsentalovich, A. N. G. Parra-Vasquez, J. Schmidt and E. Kesselman, *Nat. Nanotechnol.*, 2010, **5**, 406-411.

65. D. C. Marcano, D. V. Kosynkin, J. M. Berlin, A. Sinitskii, Z. Sun, A. Slesarev, L. B. Alemany, W. Lu and J. M. Tour, *ACS nano*, 2010, **4**, 4806-4814.
66. J. Chen, B. Yao, C. Li and G. Shi, *Carbon*, 2013, **64**, 225-229.
67. Y. Sun, Q. Wu and G. Shi, *Energy Environ. Sci.*, 2011, **4**, 1113-1132.
68. Z.-S. Wu, G. Zhou, L.-C. Yin, W. Ren, F. Li and H.-M. Cheng, *Nano Energy*, 2012, **1**, 107-131.
69. Y. Zhu, S. Murali, W. Cai, X. Li, J. W. Suk, J. R. Potts and R. S. Ruoff, *Adv. Mater.*, 2010, **22**, 3906-3924.
70. C. Soldano, A. Mahmood and E. Dujardin, *Carbon*, 2010, **48**, 2127-2150.
71. D. R. Dreyer, S. Park, C. W. Bielawski and R. S. Ruoff, *Chem. Soc. Rev.*, 2010, **39**, 228-240.
72. Y. Xu, K. Sheng, C. Li and G. Shi, *ACS nano*, 2010, **4**, 4324-4330.
73. L. Zhang and G. Shi, *J. Phys. Chem. C*, 2011, **115**, 17206-17212.
74. H. Bi, K. Yin, X. Xie, Y. Zhou, N. Wan, F. Xu, F. Banhart, L. Sun and R. S. Ruoff, *Adv. Mater.*, 2012, **24**, 5124-5129.
75. Z. Han, Z. Tang, P. Li, G. Yang, Q. Zheng and J. Yang, *Nanoscale*, 2013, **5**, 5462-5467.
76. L. Jiang and Z. Fan, *Nanoscale*, 2014, **6**, 1922-1945.
77. B. G. Choi, M. Yang, W. H. Hong, J. W. Choi and Y. S. Huh, *ACS nano*, 2012, **6**, 4020-4028.
78. Z. Zhang, F. Xiao, L. Qian, J. Xiao, S. Wang and Y. Liu, *Adv. Energy Mater.*, 2014, **4**, 1-9.
79. H. Wang, G. Wang, Y. Ling, F. Qian, Y. Song, X. Lu, S. Chen, Y. Tong and Y. Li, *Nanoscale*, 2013, **5**, 10283-10290.
80. S. Nardecchia, D. Carriazo, M. L. Ferrer, M. C. Gutiérrez and F. del Monte, *Chem. Soc. Rev.*, 2013, **42**, 794-830.
81. X. Xie, G. Yu, N. Liu, Z. Bao, C. S. Criddle and Y. Cui, *Energy Environ. Sci.*, 2012, **5**, 6862-6866.
82. Z. Chen, W. Ren, L. Gao, B. Liu, S. Pei and H.-M. Cheng, *Nat. Mater.*, 2011, **10**, 424-428.
83. J.-C. Yoon, J.-S. Lee, S.-I. Kim, K.-H. Kim and J.-H. Jang, *Sci. Rep.*, 2013, **3**, 1788, 1-8.
84. J. Yi, D. H. Lee, W. W. Lee and W. I. Park, *J. Phys. Chem. Lett.*, 2013, **4**, 2099-2104.

85. R. R. Salunkhe, Y.-H. Lee, K.-H. Chang, J.-M. Li, P. Simon, J. Tang, N. L. Torad, C.-C. Hu and Y. Yamauchi, *Chem. Eur. J.*, 2014, **20**, 13838-13852.
86. X. Huang, X. Qi, F. Boey and H. Zhang, *Chem. Soc. Rev.*, 2012, **41**, 666-686.
87. T. Kuilla, S. Bhadra, D. Yao, N. H. Kim, S. Bose and J. H. Lee, *Prog. Polym. Sci.*, 2010, **35**, 1350-1375.
88. G. Zhang, T. Wang, X. Yu, H. Zhang, H. Duan and B. Lu, *Nano Energy*, 2013, **2**, 586-594.
89. L.-Q. Mai, F. Yang, Y.-L. Zhao, X. Xu, L. Xu and Y.-Z. Luo, *Nat. Commun.*, 2011, **2**, 381, 1-5.
90. V. Subramanian, S. C. Hall, P. H. Smith and B. Rambabu, *Solid State Ionics*, 2004, **175**, 511-515.
91. X. Xie, C. Zhang, M.-B. Wu, Y. Tao, W. Lv and Q.-H. Yang, *Chem. Commun.*, 2013, **49**, 11092-11094.
92. U.M. Patil, R.R. Salunkhe, K.V. Gurav and C. Lokhande, *Appl. Surf. Sci.*, 2008, **255**, 2603-2607.
93. X.-h. Xia, J.-p. Tu, Y.-q. Zhang, Y.-j. Mai, X.-l. Wang, C.-d. Gu and X.-b. Zhao, *RSC Advances*, 2012, **2**, 1835-1841.
94. C. Zheng, C. Cao, Z. Ali and J. Hou, *J. Mater. Chem. A*, 2014, **2**, 16467-16473.
95. H. Chen, S. Zhou, M. Chen and L. Wu, *J. Mater. Chem.*, 2012, **22**, 25207-25216.
96. X. Feng, Z. Yan, N. Chen, Y. Zhang, Y. Ma, X. Liu, Q. Fan, L. Wang and W. Huang, *J. Mater. Chem. A*, 2013, **1**, 12818-12825.
97. G. Han, Y. Liu, E. Kan, J. Tang, L. Zhang, H. Wang and W. Tang, *RSC Advances*, 2014, **4**, 9898-9904.
98. S. D. Perera, A. D. Liyanage, N. Nijem, J. P. Ferraris, Y. J. Chabal and K. J. Balkus Jr, *J. Power Sources*, 2013, **230**, 130-137.
99. S. Jiang, T. Shi, H. Long, Y. Sun, W. Zhou and Z. Tang, *Nanoscale Res. Lett.*, 2014, **9**, 1-8.
100. J. Gomez, E. E. Kalu, R. Nelson, C. Akpovo, M. H. Weatherspoon, and J. P. Zheng, *ECS Electrochem. Lett.*, 2012, **1**, D25-D28.
101. X.-C. Dong, H. Xu, X.-W. Wang, Y.-X. Huang, M. B. Chan-Park, H. Zhang, L.-H. Wang, W. Huang and P. Chen, *ACS nano*, 2012, **6**, 3206-3213.
102. Y. G. Zhu, Y. Wang, Y. Shi, Z. X. Huang, L. Fu and H. Y. Yang, *Adv. Energy Mater.*, 2014, **4**, 1-8.
103. W. Deng, Y. Sun, Q. Su, E. Xie and W. Lan, *Mater. Lett.*, 2014, **137**, 124-127.

104. X. Cao, Y. Shi, W. Shi, G. Lu, X. Huang, Q. Yan, Q. Zhang and H. Zhang, *Small*, 2011, **7**, 3163-3168.
105. H. Wang, H. Yi, X. Chen and X. Wang, *J. Mater. Chem. A*, 2014, **2**, 3223-3230.
106. Y. Wei, S. Chen, D. Su, B. Sun, J. Zhu and G. Wang, *J. Mater. Chem. A*, 2014, **2**, 8103-8109.
107. V. H. Nguyen and J.-J. Shim, *J. Power Sources*, 2015, **273**, 110-117.
108. X. Dong, X. Wang, J. Wang, H. Song, X. Li, L. Wang, M. B. Chan-Park, C. M. Li and P. Chen, *Carbon*, 2012, **50**, 4865-4870.
109. Y. He, W. Chen, X. Li, Z. Zhang, J. Fu, C. Zhao and E. Xie, *ACS nano*, 2012, **7**, 174-182.
110. X. Sun, H. Wang, Z. Lei, Z. Liu and L. Wei, *RSC Advances*, 2014, **4**, 30233-30240.
111. S. Wu, W. Chen and L. Yan, *J. Mater. Chem. A*, 2014, **2**, 2765-2772.
112. U. M. Patil, J. S. Sohn, S. B. Kulkarni, H. G. Park, Y. Jung, K. V. Gurav, J. H. Kim and S. C. Jun, *Mater. Lett.*, 2014, **119**, 135-139.
113. U. M. Patil, K. V. Gurav, V. J. Fulari, C. D. Lokhande and O. S. Joo, *J. Power Sources*, 2009, **188**, 338-342.
114. C. Mondal, M. Ganguly, P. K. Manna, S. Yusuf and T. Pal, *Langmuir*, 2013, **29**, 9179-9187.
115. S. B. Kulkarni, A. D. Jagadale, V. S. Kumbhar, R. N. Bulakhe, S. S. Joshi and C. D. Lokhande, *Int. J. Hydrogen Energy*, 2013, **38**, 4046-4053.
116. K. Gurav, U. Patil, S. Shin, G. Agawane, M. Suryawanshi, S. Pawar, P. Patil, C. Lokhande and J. Kim, *J. Alloys Compd.*, 2013, **573**, 27-31.
117. X. Wang, C. Yan, A. Sumboja, J. Yan and P. S. Lee, *Adv. Energy Mater.*, 2014, **4**, 1-7.
118. J. Ji, L. L. Zhang, H. Ji, Y. Li, X. Zhao, X. Bai, X. Fan, F. Zhang and R. S. Ruoff, *ACS nano*, 2013, **7**, 6237-6243.
119. Y. Ma, W. Chen, P. Zhang, F. Teng, J. Zhou, X. Pan and E. Xie, *RSC Advances*, 2014, **4**, 47609-47614.
120. U. M. Patil, S. C. Lee, J. S. Sohn, S. B. Kulkarni, K. V. Gurav, J. H. Kim, J. H. Kim, S. Lee and S. C. Jun, *Electrochim. Acta*, 2014, **129**, 334-342.
121. U. M. Patil, M. S. Nam, J. S. Sohn, S. B. Kulkarni, R. Shin, S. Kang, S. Lee, J. H. Kim and S. C. Jun, *J. Mater. Chem. A*, 2014, **2**, 19075-19083.
122. U. M. Patil, J. S. Sohn, S. B. Kulkarni, S. C. Lee, H. G. Park, K. V. Gurav, J. H. Kim and S. C. Jun, *ACS Appl. Mater. Interfaces*, 2014, **6**, 2450-2458.

123. S. Dong, A. Q. Dao, B. Zheng, Z. Tan, C. Fu, H. Liu and F. Xiao, *Electrochim. Acta*, 2015, **152**, 195-201.
124. D. Momodu, A. Bello, J. Dangbegnon, F. Barzeger, F. Taghizadeh, M. Fabiane, A. T. C. Johnson and N. Manyala, *AIP Advances*, 2014, **4**, 1-14.
125. Y. Liu, R. Deng, Z. Wang and H. Liu, *J. Mater. Chem.*, 2012, **22**, 13619-13624.
126. H. Fan, N. Zhao, H. Wang, J. Xu and F. Pan, *J. Mater. Chem. A*, 2014, **2**, 12340-12347.
127. Z. Tai, X. Yan and Q. Xue, *J. Electrochem. Soc.*, 2012, **159**, A1702-A1709.
128. X. Dong, J. Wang, J. Wang, M. B. Chan-Park, X. Li, L. Wang, W. Huang and P. Chen, *Mater. Chem. Phys.*, 2012, **134**, 576-580.
129. D.-W. Wang, F. Li, J. Zhao, W. Ren, Z.-G. Chen, J. Tan, Z.-S. Wu, I. Gentle, G. Q. Lu and H.-M. Cheng, *ACS Nano*, 2009, **3**, 1745-1752.
130. H. Liu, Y. Wang, X. Gou, T. Qi, J. Yang and Y. Ding, *Mater. Sci. Eng., B*, 2013, **178**, 293-298.
131. K. Chen, L. Chen, Y. Chen, H. Bai and L. Li, *J. Mater. Chem.*, 2012, **22**, 20968-20976.
132. S. B. Kulkarni, U. M. Patil, I. Shackery, J. S. Sohn, S. Lee, B. Park and S. Jun, *J. Mater. Chem. A*, 2014, **2**, 4989-4998.
133. J. Zhang, J. Wang, J. Yang, Y. Wang and M. B. Chan-Park, *ACS Sustainable Chem. Eng.*, 2014, **2**, 2291-2296.
134. J. Zhang, Y. Yu, L. Liu and Y. Wu, *Nanoscale*, 2013, **5**, 3052-3057.
135. V. Varshney, S. S. Patnaik, A. K. Roy, G. Froudakis and B. L. Farmer, *ACS nano*, 2010, **4**, 1153-1161.
136. Q. Cheng, J. Tang, J. Ma, H. Zhang, N. Shinya and L.-C. Qin, *Phys. Chem. Chem. Phys.*, 2011, **13**, 17615-17624.
137. B. You, L. Wang, L. Yao and J. Yang, *Chem. Commun.*, 2013, **49**, 5016-5018.
138. M. Beidaghi and C. Wang, *Adv. Funct. Mater.*, 2012, **22**, 4501-4510.
139. Y. S. Moon, D. Kim, G. Lee, S. Y. Hong, K. K. Kim, S. M. Park and J. S. Ha, *Carbon*, 2015, **81**, 29-37.
140. Y. Zhang, M. Ma, J. Yang, W. Huang and X. Dong, *RSC Advances*, 2014, **4**, 8466-8471.
141. Z. Fan, J. Yan, L. Zhi, Q. Zhang, T. Wei, J. Feng, M. Zhang, W. Qian and F. Wei, *Adv. Mater.*, 2010, **22**, 3723-3728.

142. Z. Yan, L. Ma, Y. Zhu, I. Lahiri, M. G. Hahm, Z. Liu, S. Yang, C. Xiang, W. Lu, Z. Peng, Z. Sun, C. Kittrell, J. Lou, W. Choi, P. M. Ajayan and J. M. Tour, *ACS Nano*, 2013, **7**, 58-64.

143. V. Sridhar, H.-J. Kim, J.-H. Jung, C. Lee, S. Park and I.-K. Oh, *ACS nano*, 2012, **6**, 10562-10570.

144. Y. Zhu, L. Li, C. Zhang, G. Casillas, Z. Sun, Z. Yan, G. Ruan, Z. Peng, A.-R. O. Raji and C. Kittrell, *Nat. Commun.*, 2012, **3**, 1225.

145. J. Lin, C. Zhang, Z. Yan, Y. Zhu, Z. Peng, R. H. Hauge, D. Natelson and J. M. Tour, *Nano Lett.*, 2012, **13**, 72-78.

146. F. Du, D. Yu, L. Dai, S. Ganguli, V. Varshney and A. Roy, *Chem. Mater.*, 2011, **23**, 4810-4816.

147. J. Liu, L. Zhang, H. B. Wu, J. Lin, Z. Shen and X. W. Lou, *Energy Environ. Sci.*, 2014, **7**, 3709-3719.

148. G. Zhu, Z. He, J. Chen, J. Zhao, X. Feng, Y. Ma, Q. Fan, L. Wang and W. Huang, *Nanoscale*, 2014, **6**, 1079-1085.

149. J. Yan, Z. Fan, W. Sun, G. Ning, T. Wei, Q. Zhang, R. Zhang, L. Zhi and F. Wei, *Adv. Funct. Mater.*, 2012, **22**, 2632-2641.

150. H. Wang, Y. Liang, T. Mirfakhrai, Z. Chen, H. S. Casalongue and H. Dai, *Nano Research*, 2011, **4**, 729-736.

151. A. D. Jagadale, V. S. Kumbhar, D. S. Dhawale and C. D. Lokhande, *Electrochim. Acta*, 2013, **98**, 32-38.

152. C.-T. Hsu, C.-C. Hu, T.-H. Wu, J.-C. Chen and M. Rajkumar, *Electrochim. Acta*, 2014, **146**, 759-768.

Figure caption:

Figure 1: Applicability of 3D graphene based electrode materials in numerous devices.

Figure 2: Schematic representation of graphene synthesis processes by (a) "Bottom-up" and (b) "Top-down" approach.

Figure 3: Schematic for fabrication process of 3D graphene foam (a) Self-assembly of 3D graphene by chemical method, (b) Template assisted 3D graphene synthesis by chemical method, (c) Template assisted 3D graphene synthesis by CVD method.

Figure 4: (a) Various pseudocapacitive materials (PCMs) viz. metal oxides/hydroxides, polymers grown on 3D GF as supercapacitor electrodes (b) Schematic growth mechanism of PCMs nanostructures on 3D GF by self-assembly and oriented attachment process.

Figure 5: Structural (a) Raman, (b) XRD and morphological properties (c-e) SEM images of 1D nanostructured MnO_2/GF. (f) Comparative CV curves of MnO_2/GF, MnO_2/CC and GF electrode (g) CV curves at different scan rate for MnO_2/GF, (h) scan rate dependent specific capacitance of MnO_2/GF and MnO_2/CC electrodes in 1M Na_2SO_4.

Figure 6: (a-c) SEM images of $Ni(OH)_2$ grown over GF. (d) Comparative CV curves of $Ni(OH)_2$/GF and $Ni(OH)_2$/SS (e) CV curves at different scan rate for $Ni(OH)_2$/GF (f) scan rate dependent specific capacitance of $Ni(OH)_2$/GF and $Ni(OH)_2$/SS electrodes in 1M KOH.

Figure 7: (a, b) SEM, (c) TEM images of CBD grown $Co(OH)_2$ nanorods on GF. (d) CV curves at different scan rates in 1M KOH (e) galvanostatic charge-discharge (GCD) plots at various current densities of $Co(OH)_2$/GF electrode. (f) Current densities dependent specific capacitance of $Co(OH)_2$/GF and $Co(OH)_2$/SS electrodes. (g-h) SEM, (i) TEM images of PED grown $Co(OH)_2$ flakes on GF. (j) Comparative CV curves of $Co(OH)_2$/GF and $Co(OH)_2$/SS (k) GCD plots at various current densities of $Co(OH)_2$/GF electrode. (l) Current densities dependent specific capacitance of $Co(OH)_2$/GF in 1M KOH.

Figure 8: (a-e) Composition influenced morphological transformation of CBD grown $Co_xNi_{1-x}(OH)_2$ MMH on GF. Composition dependent (f) CV curves, (g) GCD curves and (h) specific capacitance of $Co_xNi_{1-x}(OH)_2$/GF electrode for different Ni (x) content in 1M KOH.

Figure 9: (a-c) SEM images of CBD grown nanofibers PANI on GF. (d) XRD of semi-crystalline PANI; Inset shows photograph of PANI/GF electrode. Comparative (e) CV curves and (f) GCD curves and (g) Nyquist plot of PANI/GF and PANI/SS electrodes in 1M H_2SO_4, respectively. Inset of (g) shows graph of current dependent coulombic efficiency and Ragone plot.

Figure 10: (a) Schematic presentation of CNT growth on GF by CVD method followed by MnO_2 deposition by chemical method. (b) Raman and (c) XRD analysis to confirm the formation of MnO_2/CNT/GF electrode. (d) SEM images of chemically grown MnO_2 nanoflakes on GF. Comparative (e) CV curves of graphene/Ni foam, CNTs/Graphene/Ni

foam, MnO_2/CNTs/Graphene/Ni foam and (f) capacitive performance against ESR with other reported work. (Reproduced from Ref. 148. Copyright 2014 Royal society of chemistry).

Figure 11: (a) Schematic of symmetric/asymmetric supercapacitor devices, (b) Demonstration of practical application of PCMs/GF ($Co(OH)_2$/GF) based symmetric devices we used to run the toy fan and glow LED, (c) Ragone plot of PCMs/GF based devices summarizing with high-end commercial supercapacitor devices.

Figure 12: (a) Demonstration of charge transport mechanism for PCM/MCC, PCM-GO/MCC and PCM/GF (b) Combination of CNTs and GF to overcome the space limited effective surface area by planar (2D) geometry of GF.

Table 1. Summary of capacitive performances for Metal oxide/GF electrodes in supercapacitors.

Table 2. Summary of capacitive performances for Metal hyoxide/GF electrodes in supercapacitors.

Table 3. Summary of capacitive performances for conducting polymers/GF electrodes in supercapacitors.

Table 4. Summary of capacitive performances for PCMs coated CNTs/GF electrodes in supercapacitors.

Table 5. Summary of capacitive performances for symmetric and asymmetric supercapacitors devices.

Figures

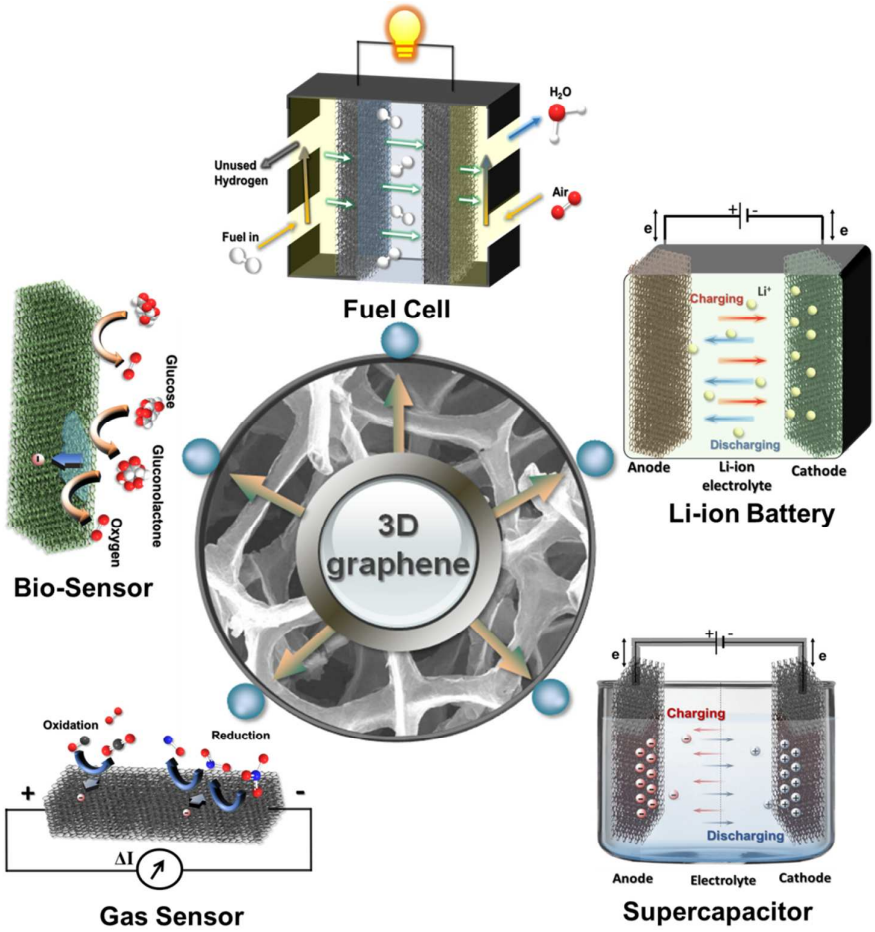

Figure 1

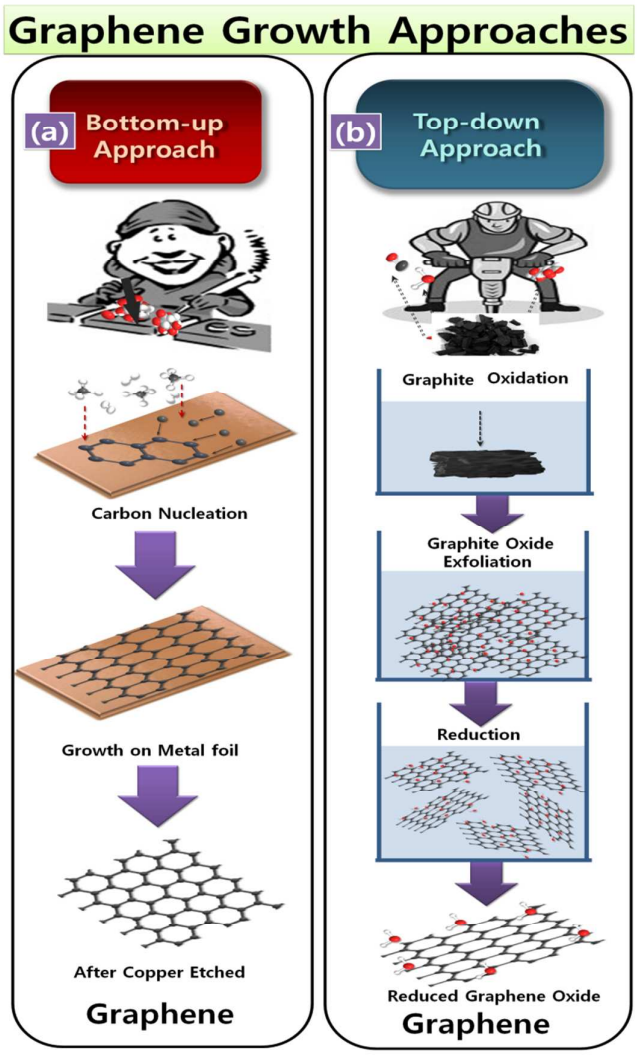

Figure 2

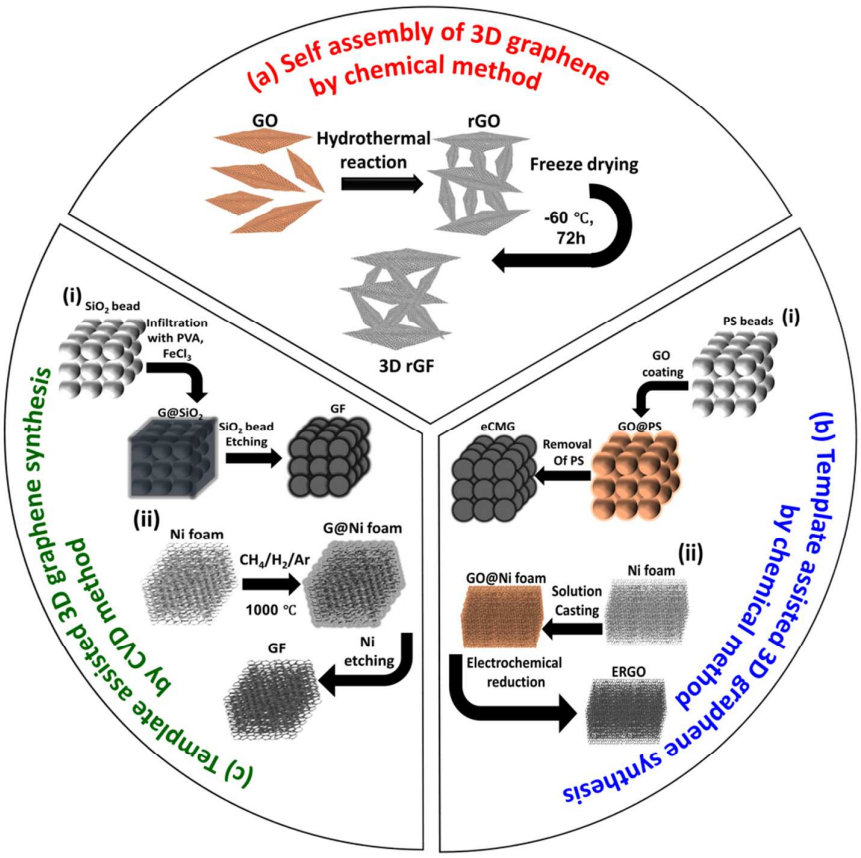

Figure 3

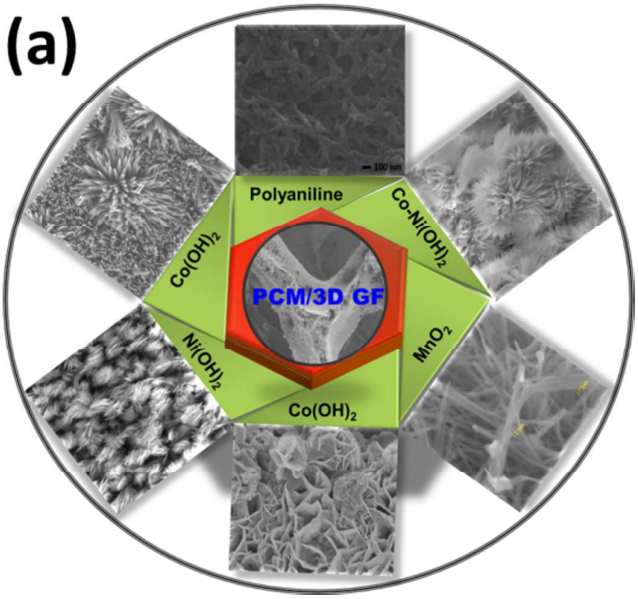

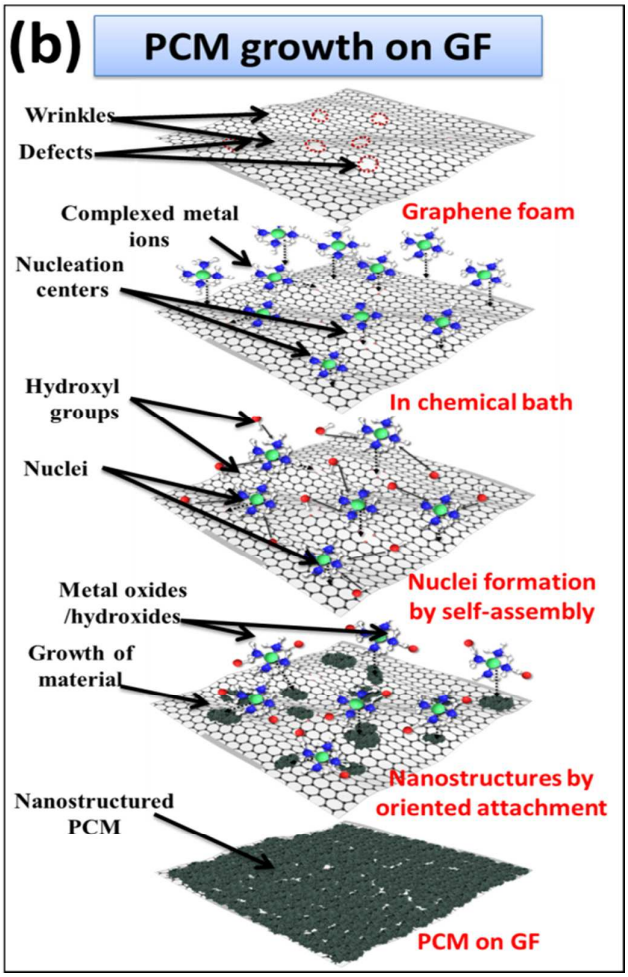

Figure 4

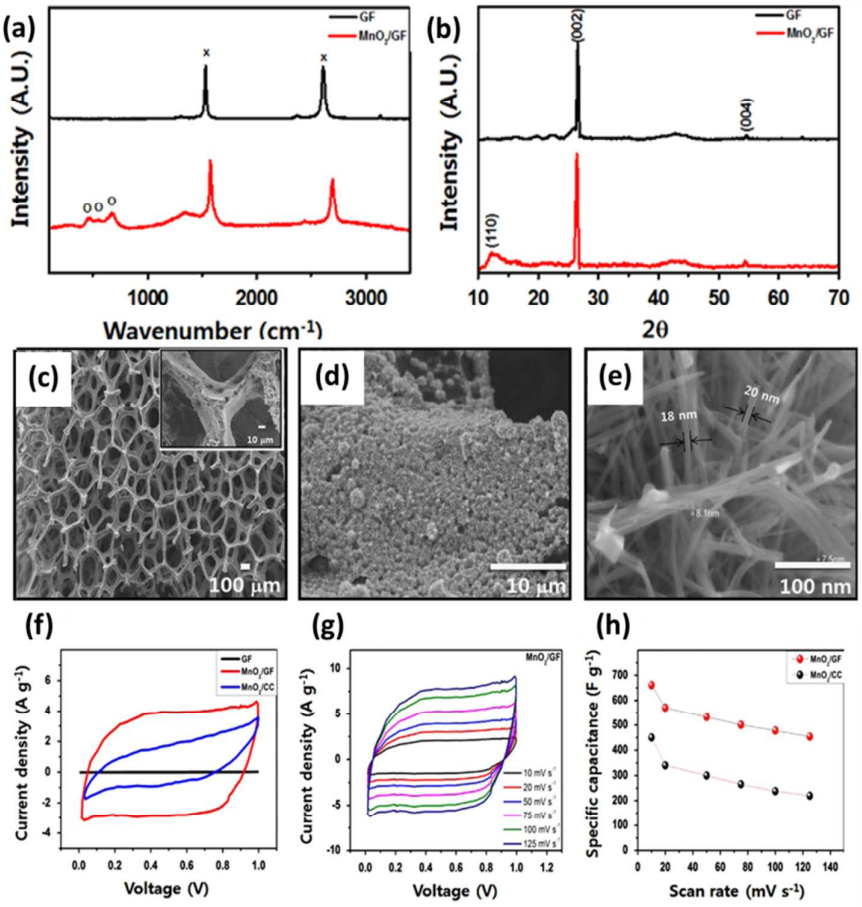

Figure 5

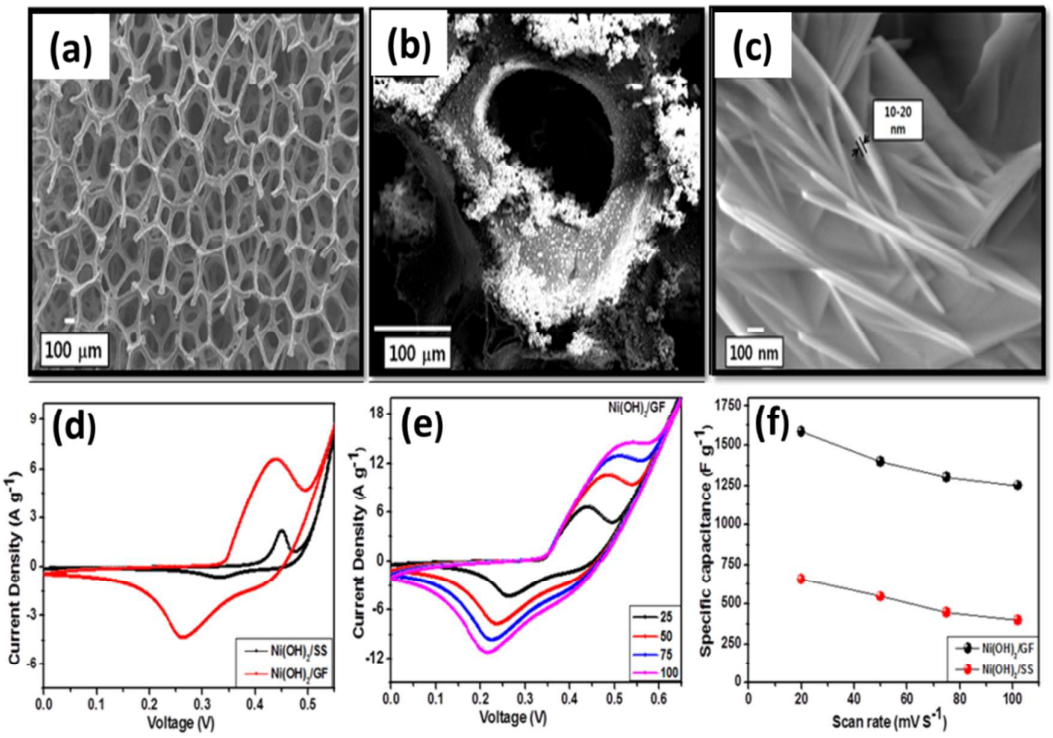

Figure 6

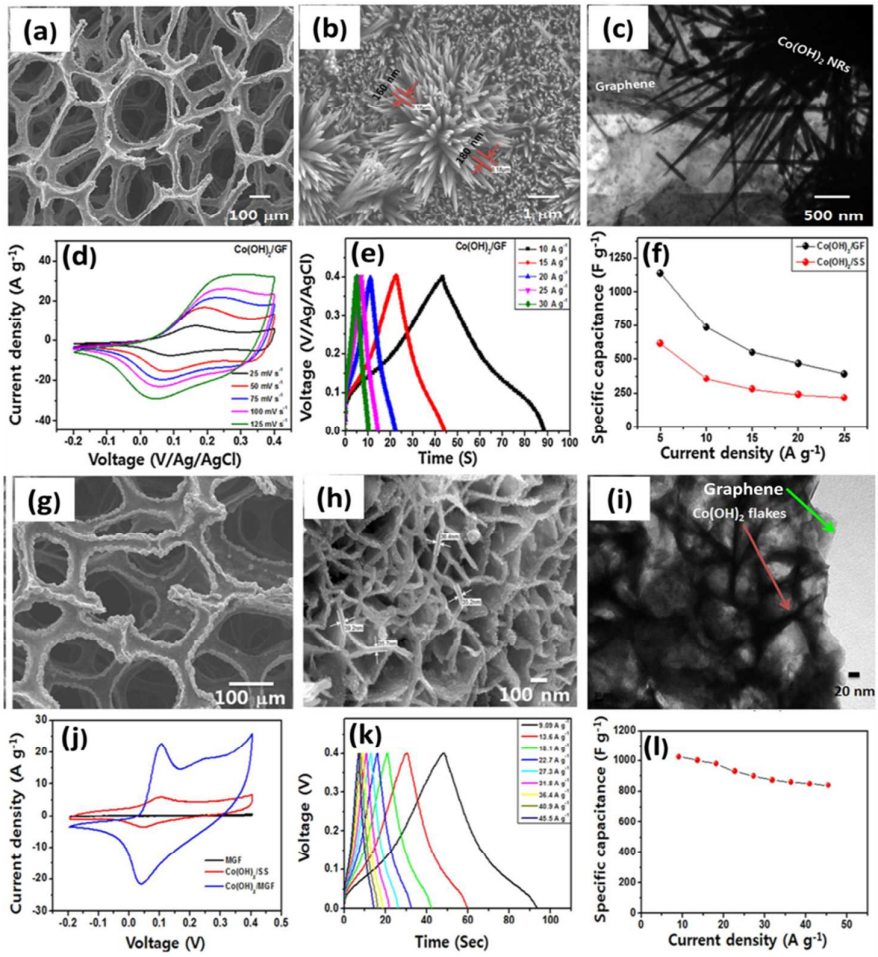

Figure 7

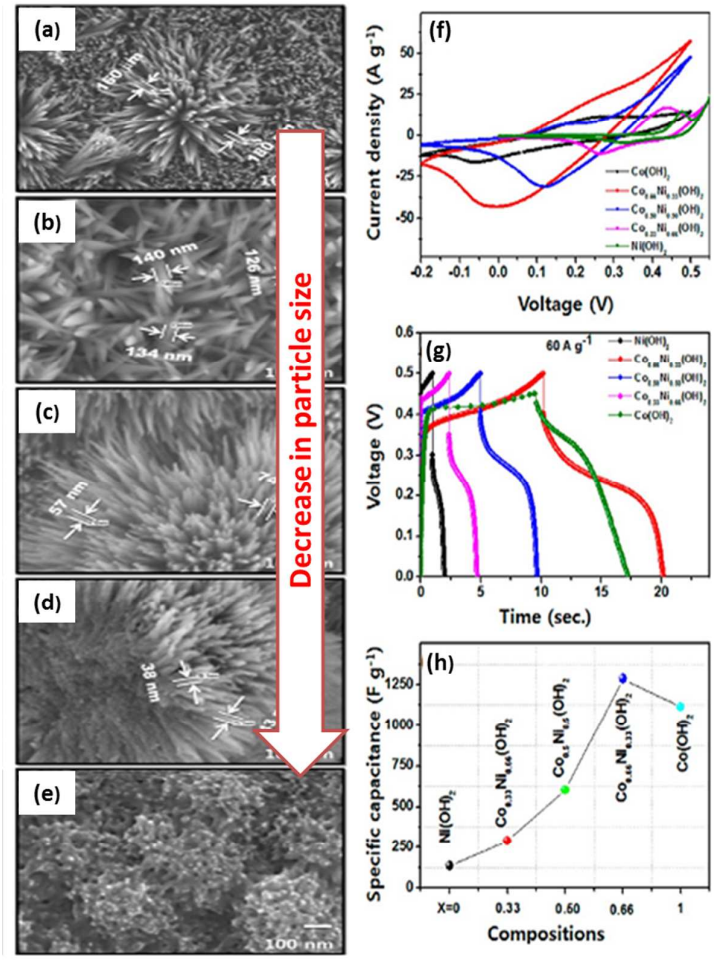

Figure 8

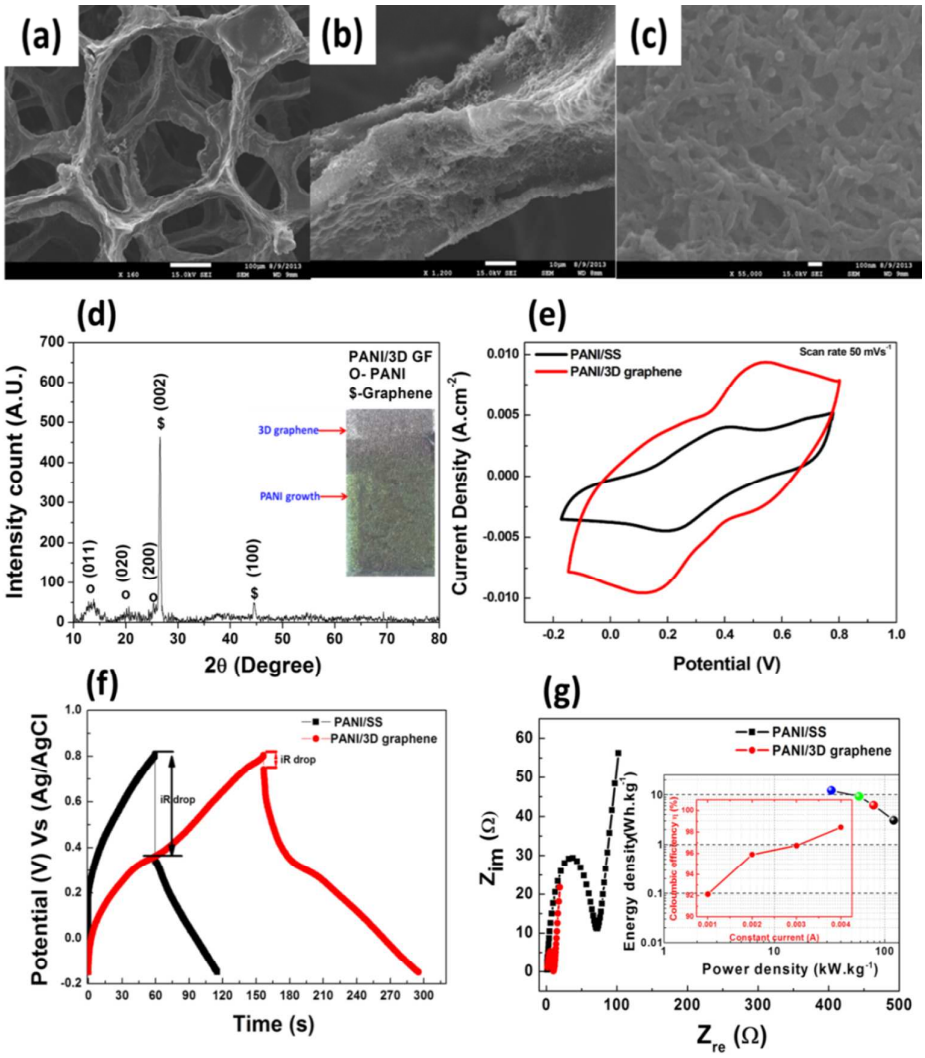

Figure 9

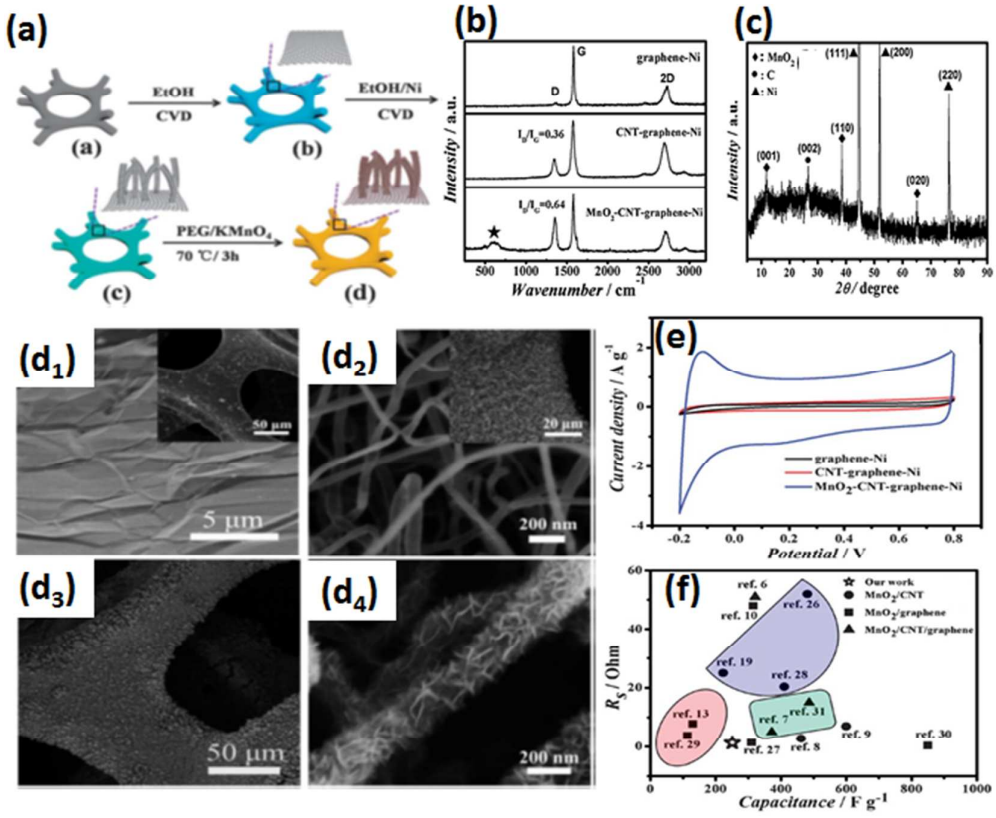

Figure 10

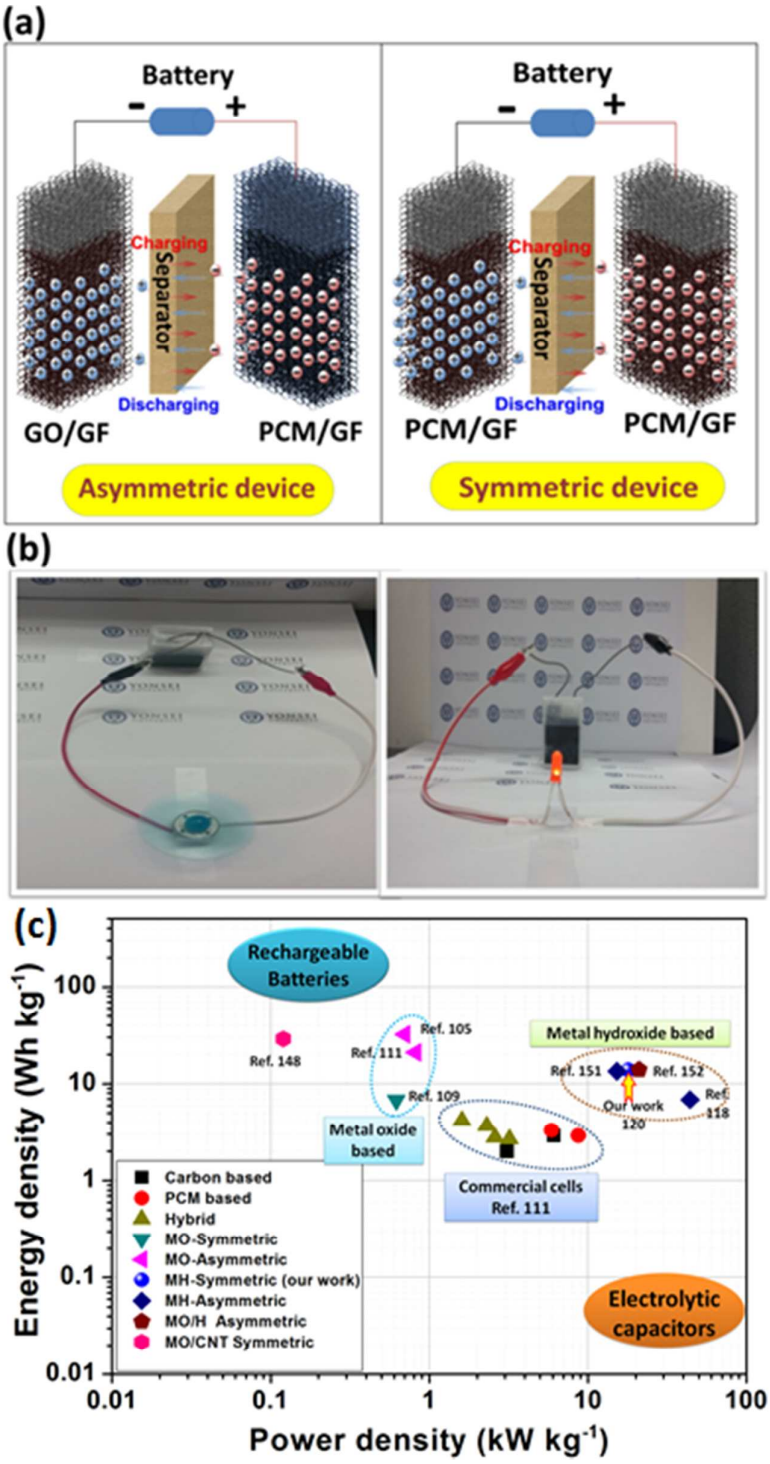

Figure 11

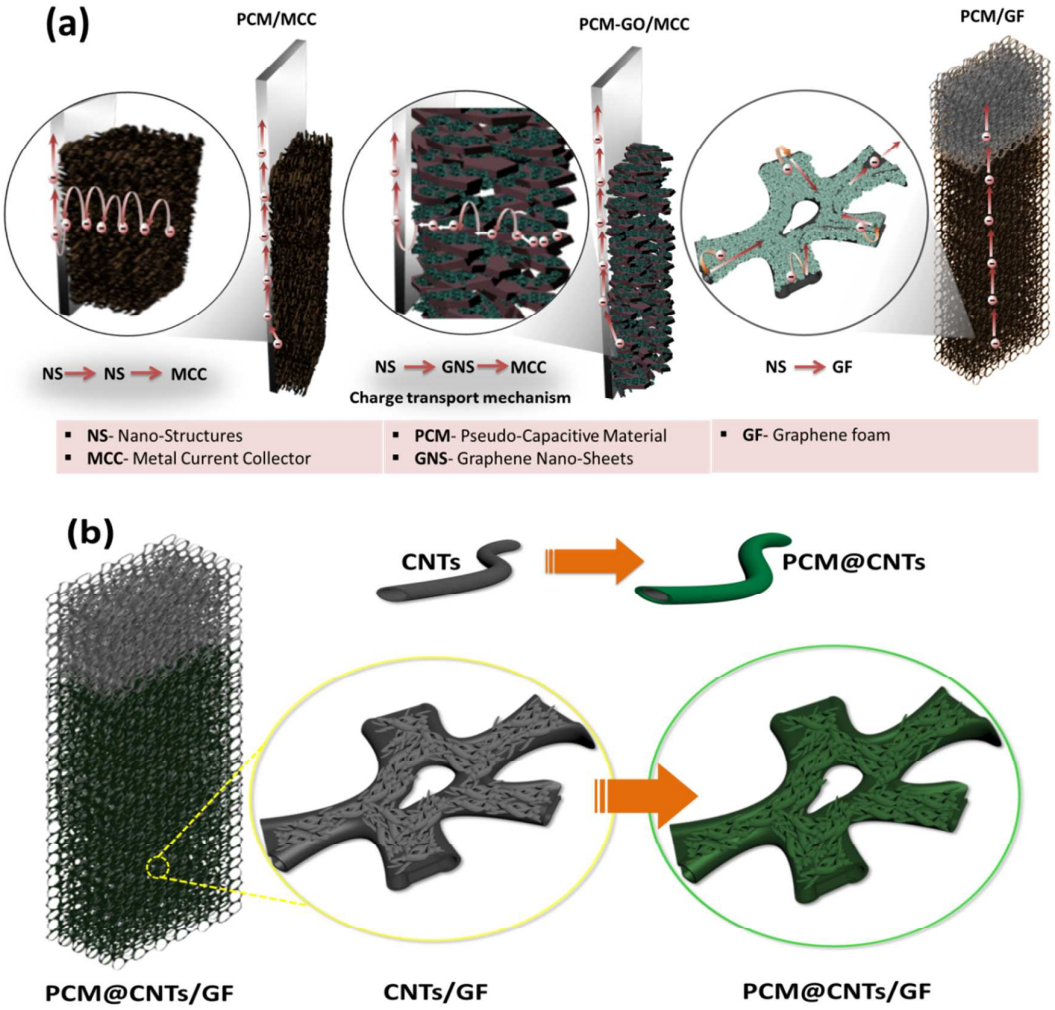

Figure 12

Materials on 3DGF	Synthesis methods	Morphology	Cell type	Specific capacitance/Considered mass	Stability	Ref
Co_3O_4	Hydrothermal synthesis	Nanowire	Three electrodes system (Ag/AgCl - Pt foil)	1100 F g^{-1} (10 A g^{-1}) Mass of active material	500 cycles	101
CoO	Hydrothermal synthesis	Nanorod	Three electrodes system (Hg/HgO - Pt)	980 F g^{-1} (1 A g^{-1}) Mass of active material	10000 cycles (103%)	102
CoO	Hydrothermal method and thermal treatment	Nanobundle	Three electrodes system (Hg/HgO - Pt plate)	352.7 F g^{-1} (1 A g^{-1}) Total mass of electrodes	1000 cycles	103
NiO	Electrochemical deposition	Porous film	Three electrodes system (Ag/AgCl - Pt wire)	816 F g^{-1} (5 mV s^{-1}) Mass of active material	2000 cycles	104
NiO	Pulsed laser deposition	Nanoparticle	Three electrodes system (Hg/HgO - Pt foil)	1225 F g^{-1} (2 A g^{-1}) Mass of active material	1000 cycles (89%)	105
$NiCo_2O_4$	Hydrothermal method	Mesoporous nanosheet	Three electrodes system (SCE – Pt wire)	778 F g^{-1} (1 A g^{-1}) Mass of active material	10000 cycles	106
$NiCo_2O_4$	Electrodeposition	Nanoparticles	Three electrodes system (SCE - Pt plate)	2260 F g^{-1} (1 A g^{-1}) Mass of active material	10000 cycles (92.8%)	107
MnO_2	Hydrothermal method	Various shape (flower-like, nano-bush, reticular, nanotube structure)	Three electrodes system (Ag/AgCl - Pt plate)	560 F g^{-1} (0.2 A g^{-1}) Mass of active material	1000 cycles (79%)	108
MnO_2	Electrochemical deposition	Nanosheet	Three electrodes system (Ag/AgCl - Pt wire)	465 F g^{-1} (2 mV s^{-1}) Mass of active material	5000 cycles	109
MnO_2	Hydrothermal method	Nanoflake	Three electrodes system (Ag/AgCl - Pt foil)	210 F g^{-1} (2 A g^{-1}) Mass of active material	4000 cycles (75%)	110

MnO_2	Reduction-induced in situ self-assembly	Nanoparticle	Three electrodes system (Ag/AgCl - Pt foil)	242 F g^{-1} (1 A g^{-1}) Mass of active material	1000 cycles (89.6%)	111
MnO_2	Solution growth method	Nanofiber	Three electrodes system (Ag/AgCl - Pt wire)	670 F g^{-1} (10 mVs^{-1}) Mass of active material	-	112

Table 1.

Materials on 3DGF	Synthesis methods	Morphology	Cell type	Specific capacitance/Considered mass	Stability	Ref
$Ni(OH)_2$	Hydrothermal reaction	Micro-flakes	Three electrodes system (Ag/AgCl - Pt mesh)	1.56 X 10^3 F g^{-1} (0.5 A g^{-1}) Mass of active material	1000 cycles (65%)	118
			Three electrodes system (Ag/AgCl - Pt mesh)	166 F g^{-1} (0.5 A g^{-1}) Total mass of electrode	10000 cycles (63.2%)	
$Ni(OH)_2$	Chemical method	Nanoflakes	Three electrodes system (Ag/AgCl - Pt wire)	1568 F g^{-1} (20 mVs^{-1}) Mass of active material	-	Not Published
$Ni(OH)_2$	Hydrothermal method	Nanosheet	Three electrodes system (Ag/AgCl - Pt mesh)	2860 F g^{-1} (2 A g^{-1}) Mass of active material	1000 cycles (65%)	119
$Co(OH)_2$	Chemical bath deposition	Nanorod	Three electrodes system (Ag/AgCl - Pt mesh)	1138 F g^{-1} (10 A g^{-1}) Mass of active material	1000 cycles (74%)	120
$Co(OH)_2$	Electrodeposition	Microflake	Three electrodes system (Ag/AgCl - Pt mesh)	1030 F g^{-1} (9.09 A g^{-1}) Mass of active material	5000 cycles (94%)	121
$Co_xNi_{1-x}(OH)_2$	Chemical bath deposition	Nanorod	Three electrodes system (Ag/AgCl - Pt mesh)	1847 Fg^{-1} (5 A g^{-1}) Mass of active material	1000 cycles (64%)	122
$Ni_xCo_{2x}(OH)_{6x}$	Electrodeposition	Nanoflake	Three electrodes system (Ag/AgCl - Pt foil)	703.6 mF cm^{-2} (10 mA cm^{-2})	1000 cycles (97.5%)	123
NiAl double hydroxide	Solvothermal synthesis	Microsphere	Three electrodes system (Ag/AgCl - Glassy carbon plate)	1252 F g^{-1} (1 A g^{-1})	1000 cycles (97%)	124

Table 2.

Materials on 3DGF	Synthesis methods	Morphology	Cell type	Specific capacitance/ Considered mass	Stability	Ref
PANI	In-situ polymerization	Nanofiber	Three electrodes system (SCE - Pt wire)	334 F g^{-1} (2 A g^{-1}) Total mass of electrode	5000 cycles	127
PANI	In-situ polymerization	Nano-square	Three electrodes system (Ag/AgCl - Pt wire)	346 F g^{-1} (4 A g^{-1}) Mass of active material	600 cycles (70.8%)	128
PANI	In-situ polymerization	-	Three electrodes system (Ag/AgCl - Pt wire)	233 F g^{-1} (2 mV s^{-1}) Mass of active material	1500 cycles	129
PANI	In-situ anodic electropolymerization	Belt-like	Three electrodes system (SCE – Pt foil)	463 F g^{-1} (1 mV s^{-1}) Mass of active material	500 cycles (90.6%)	130
PANI	Electrochemical polymerization	Fiber	Three electrodes system (SCE - Pt foil)	716 F g^{-1} (0.47 Ag^{-1}) Total mass of electrode	500 cycles	131
PANI	Chemical oxidative polymerization	Nanofiber	Three electrodes system (Ag/AgCl - Pt foil)	1024 F g^{-1} (10 mV s^{-1}) Mass of active material	5000 cycles (86.5%)	132
PANI	Electrodeposition	Porous nanofibers	Three electrodes system (Ag/AgCl - Pt plate)	1.7 F cm^{-2} (1 mA cm^{-2}) Total area of electrode	5000 cycles (69%)	133
PPy	Chemical polymerization	Hollow sphere	Three electrodes system (Ag/AgCl - Pt sheet)	500 F g^{-1} (5 A g^{-1}) Total mass of electrode	10000 cycles	134

Table 3

Materials on 3DGF	Synthesis methods	Morphology	Cell type	Specific capacitance/Considered mass	Stability	Ref.
MnO_x/(COOH) CNT/GF	Hydrothermal/Hydrothermal/ CVD	-	Two electrodes system	0.32 mF cm^{-2} (2 V s^{-1})/Total area of electrode	10000 cycles (89.5%)	139
Mn_2O_3/CNT/GF	Electrodeposition/Electrodepo sition/CVD	Nanowires/rods	Three electrode system (Ag/AgCl – Pt plate)	370 F g^{-1} (100 mA g^{-1})/Mass of active material	1000 cycles	140
$Ni(OH)_2$/CNT/ GF	Electrodeposition/CVD/Chemi cal method	Nanoflakes/rods	Three electrodes system (SCE - Pt plate)	1384 F g^{-1} (4 A g^{-1})/Mass of active material 970 F g^{-1} (4 A g^{-1})/Mass of total electrode	20,000 (99%)	146
MnO_2/CNT/GF	Hydrothermal/CVD/CVD	Nanosheets/rods	Two electrodes system	0.8 F cm^{-2}/Total area of electrode	-	147
MnO_2/CNT/GF	Chemical method/CVD/CVD	Nanoflakes/rods	Two electrodes system	251 F g^{-1} (1 A g^{-1})/Mass of total electrode	3000 cycles (82%)	148

Table 4

Materials on 3DGF	Synthesis methods	Morphology	Cell type	Specific capacitance	Stability	Ref.
MnO_2	Electrodeposition	Nanosheets	Two electrodes system (Symmetric devices)	130 F g^{-1} (2 mV s^{-1})/Total mass of device	5000 cycles (82%)	109
MnO_2	Hydrogel	Nanoparticle	Two electrodes system (Asymmetric devices)	59 F g^{-1} (1 A g^{-1})/Total mass of device	1000 cycles (90%)	111
$Co(OH)_2$	Chemical method	Nanorod	Two electrodes system (Symmetric devices)	69 F g^{-1} (5 A g^{-1})/Total mass of device	1000 cycles (74%)	120
NiO	PLD process	Nanotube	Two electrodes system (Asymmetric devices)	116 F g^{-1} (1 A g^{-1})/Mass of two electrodes active material	2000 cycles (94%)	105
$Ni(OH)_2$	Hydrothermal reaction	Microflakes	Two electrodes system (Asymmetric devices)	119 F g^{-1} (1 A g^{-1})/Mass of two electrodes active material	10000 cycles (63.2%)	118
MnO_x/(COOH) CNT	Hydrothermal reaction		Two electrodes system (Symmetric devices)	0.32 mF cm^{-2} (2 V s^{-1})/Total area of electrode	10000 cycles (89.5%)	139
MnO_2/CNT	Chemical method	Nanoflakes/rods	Two electrodes system (Symmetric devices)	251 F g^{-1} (1 A g^{-1})/Mass of total electrode	3000 cycles (82%)	148

Table 5